



universität  
wien

# MASTERARBEIT / MASTER'S THESIS

Titel der Masterarbeit / Title of the Master's Thesis

„Synthesis and characterization of novel 5,8-dihydroindolo[2,3-*d*]benzazepin-7(6*H*)-ones and their metal complexes as potential anticancer drugs“

verfasst von / submitted by

Christopher Wittmann BSc

angestrebter akademischer Grad / in partial fulfilment of the requirements for the degree of  
Master of Science (MSc)

Wien, 2019 / Vienna 2019

Studienkennzahl lt. Studienblatt /  
degree programme code as it appears on  
the student record sheet:

A 066 862

Studienrichtung lt. Studienblatt /  
degree programme as it appears on  
the student record sheet:

Masterstudium Chemie

Betreut von / Supervisor:

ao. Univ.-Prof. Dr. Vladimir Arion



## Acknowledgement

I want to thank all the people who helped me during my work on this master thesis:

Ao. Univ.-Prof. Dr. Vladimir Arion for the excellent supervision and patience during the work as well as for improvement of my theoretical and practical knowledge.

Dr. Felix Bacher, Bakk. MSc for the supervision in the laboratory as well as for the constant exchange and improvement of my knowledge.

Prof. Ing. Peter Rapta, DrSc. for the collaboration in the field of electrochemistry.

Dr. Gabriella Spengler for the investigation of the cytotoxicity of the drugs synthesised.

Ao. Univ.-Prof. Mag. Dr. Markus Galanski, Ass.-Prof. Mag. Dr. Hanspeter Kählig, Ing. Susanne Felsing, Ricarda Bugl and Sabine Schneider for the measurements of one and two dimensional NMR spectra.

Ing. Alexander Roller and his team and Univ.-Prof. Mag. Dr. Gerald Giester for the X-ray diffraction measurements.

Mag. Johannes Theiner for performing the elemental analyses.

Mag. Elfriede Limberger for the help with diverse administrative concerns.

Eva Rasch BSc for the supply of every kind of material.

Ass.-Prof. Dr. Peter Unfried for permanent exchange regarding thermogravimetric analyses and IR spectroscopy.

All colleagues from the Institute of Inorganic Chemistry at the University of Vienna, especially Dr. Felix Bacher, Bakk. MSc, Kateryna Ohui, BSc MSc. Mag. Dr. Miljan Milunovic, MSc, Dr. Iryna Stepanenko and Valentin Fuchs, BSc MSc, for the excellent working atmosphere.

o. Univ.-Prof. Dr. Dr. Bernhard Keppler for the opportunity to work at the Institute of Inorganic Chemistry of the University of Vienna.



## Abstract

In the past century the treatment of cancer has improved rapidly. The metal based anticancer therapy was set by cisplatin. This drug and many other platinum(II) drugs were and are currently used to treat cancer. Nevertheless, these drugs show severe side effects. More promising are ruthenium(II)- or ruthenium(III)-based drugs to further reduce side effects and overcome acquired resistance against cisplatin. Although these drugs work well, improvement is still needed in synthesising targeted drugs.

Two major protein groups controlling the cell's proliferation are cyclin-dependent kinases (CDKs) and tubulins. Many different sub-classes of CDKs are known. Some of them are sentinels of the cell cycle allowing the cell to proliferate. This enzyme is corrupted in cancer, thus, no monitoring for damaged DNA can be conducted, allowing the cell to proliferate with an accumulation of mutations. Therefore, targeted inhibition of these aberrant proteins may lead to cell cycle arrest. Tubulin plays the main role during mitosis. It polymerises at the beginning and depolymerises when the separation of chromosomes is finished. Thus, targeted inhibition of either the polymerisation or depolymerisation of this protein complex will stop the cell from proliferating.

With the discovery of the highly cytotoxic effects of paullones and its derivatives, CDKs could be targeted to eliminate aberrant cells. The drawback of these molecules is their low aqueous solubility, which was successfully improved by complex formation with different metals like copper(II) or iron(III). Latonduine derivatives bearing an indole moiety have promising tubulin inhibitory properties, but suffer from the same disadvantage as paullones.

In this work, latonduine derivatives, namely 5,8-dihydroindolo[2,3-*d*][2]benzazepine-7(6*H*)-ones, were synthesised and modified by creating suitable metal binding sites for accommodation of copper(II) and of iron(III). The ligands were characterised by one- and two-dimensional  $^1\text{H}$  and  $^{13}\text{C}$  NMR spectroscopy, UV-vis and IR spectroscopy, elemental analysis and electrochemical techniques. Preliminary cytotoxicity assays will indicate high potential for their further development as anticancer drugs.



# Table of Contents

Acknowledgement.....	I
Abstract.....	III
1. Introduction.....	1
1.1. Cancer diseases in Austria.....	1
1.2. Early cancer research.....	6
1.3. Status quo of cancer research.....	8
2. Cancer treatment.....	17
2.1. Transition metal complexes and their clinical use.....	17
2.1.1. Platinum.....	17
2.1.2. Ruthenium.....	19
2.1.3. Copper.....	20
2.1.4. Iron.....	21
2.2. CDKs and CDK inhibitors.....	22
2.3. Tubulin and tubulin-inhibitors.....	25
2.4. Indolobenzazepines.....	28
2.5. Metal complexes with paullone derived ligands.....	32
3. Experimental part.....	34
3.1. Synthesis of 5,8-dihydroindolo[2,3-d][2]benzazepin-7(6H)-one.....	34
3.2. Synthesis of proligands.....	38
3.3. Synthesis of metal complexes.....	42
4. Results and Discussion.....	44
4.1. Synthesis of the organic scaffolds.....	44
4.2. Copper(II) complexes.....	46
4.3. Iron(III) complexes.....	49
4.4. UV-vis measurements.....	50
4.5. Electrochemical behaviour.....	51
5. Conclusion.....	57
6. References.....	58
7. Supplementary Information.....	i
7.1. Zusammenfassung.....	i
7.2. Abstract.....	ii

# 1. Introduction

## 1.1. Cancer diseases in Austria

It is well known that the older the society is the more affected it is by various diseases. Cancer is a major concern in the health service system. In Austria the incidences of cancer diseases are documented by the Statistik Austria,<sup>1,2</sup> while the surveillance of the whole world is done by the World Health Organisation (WHO).<sup>3</sup> It should be noticed that not only adults but, unfortunately, also children are frequently diagnosed with cancer.<sup>4</sup> The growing number of people diagnosed with cancer is of large concern. While in 1983, 29349 persons in Austria were diagnosed with cancer, this number rose to 31427 in only 5 years. Within the last years, this number increased further, reaching the point of around 40000 new incidences of cancer in 2015.<sup>2</sup>

Another worthy of noting fact is that women were more often diagnosed with cancer than men until 1997. In the following years, this trend turned upside-down and men were diagnosed with cancer more often. In fact, women are not less diagnosed with cancer since 1997 but the number does not rise as fast as the reported diseases affecting men. It is also of note that, although men were far more often diagnosed with cancer since the late 1990s, it can be seen from Figure 1 that no difference in the frequency of diagnoses is observed when comparing men and women.<sup>2</sup> Figure 1 shows the incidences of cancer. The reasons are not clear since the demographic evolution of men and women did not differ.<sup>5</sup> One reason could be prophylactic medical examinations, which are more promoted for women in Austria than for men.

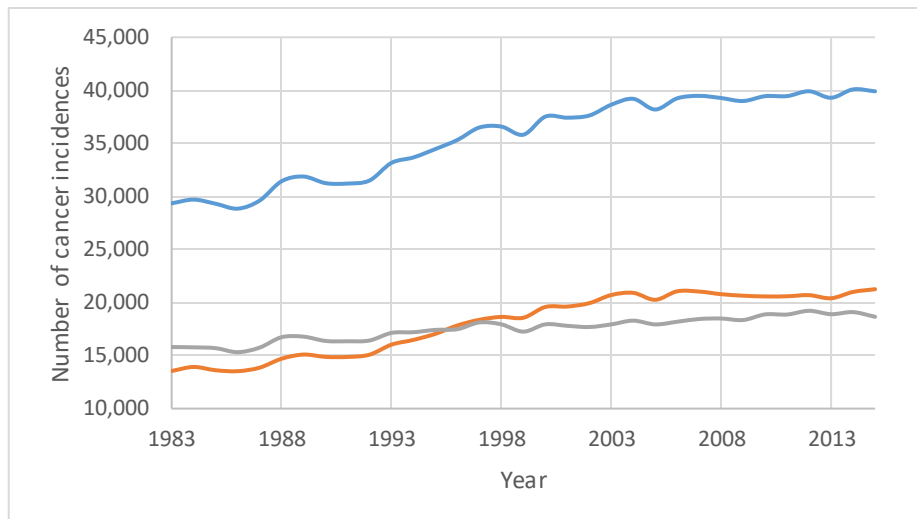


Figure 1: Overview of the annually newly registered cancer incidents; red represents the men, green represents the women, blue represents the total amount.<sup>2</sup>

It is also worth noting that cancer may be detected at different stages of tumour growth. While sometimes it is detected as an early stage of disease, it is also possible that, to a certain extent, the malign tissue will be recognised only after the metastatic spread or even after death. From 2013 to 2015 research was conducted on this field<sup>6</sup> showing that every third diagnosis is done at the localised stadium of cancer growth and half of the newly diagnosed cases are limited to a certain area (localised and regionalised diseases). Nevertheless, cases are reported where cancer was detected only after dissemination or metastasis. Combined with the findings of systemic cancer disease in the human body, these incidences sum up to 20%.<sup>6</sup> What is remarkable, is that there are also cases where the stage of incidence is not known (see Figure 2).

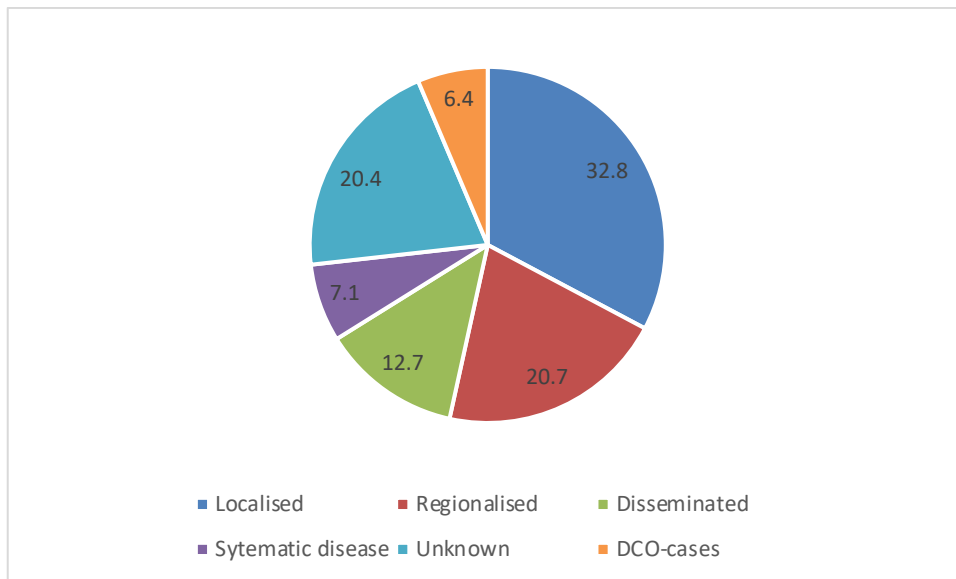


Figure 2: Overview of the different phases cancer while being detected; the numbers are given in %, DCO stands for death certificate only<sup>6</sup>

The prognosis for future incidences of cancer follows the trend, which was observed up to now. The total amount of newly diagnosed people will rise as the population in Austria becomes older. This is due to the progressive ageing of the “Baby-Boom-Generation” (the generation born in the 1960s and 1970s). All these people are slowly becoming older, and their risk of developing cancer is also increasing.<sup>7</sup> Surprisingly, not all cancer diseases show a growing trend. Certain types of cancer seem to decrease with time. Examples are gastric, ovarian and bladder cancer, as well as prostate and cervical cancer. Their decrease is presumably due to the medicinal progress and sustainable provision.<sup>7</sup>

When considering the incidences of cancer in Austria, one also has to take into account the prevalence of cancer kind. Since 2001 the prevalence was rocketing from 203.466 to 340.840 cancer cases in 2015 with more women suffering from cancer than men during the whole period.<sup>8</sup> Furthermore, the prevalence in observed locations differs dramatically between men and women. According to statistics conducted in 2015,<sup>9</sup> men are most often diagnosed with prostate tumour, whereas women suffer mostly from breast tumour. Regarding tissues both genders have in common, breast cancer and thyroid cancer are mainly found in women, whereas bladder cancer and cancerous tissues in the head and neck area, especially pharyngolaryngeal cancer, occur more often in men.<sup>9</sup>

The prognosis for the prevalence of cancer was also calculated by Statistik Austria.<sup>10</sup> It is stated that by the end of 2014, 3.83% of the Austrian population was diagnosed with cancer, whereas

the number of women was slightly higher than the number of men. The calculations show, considering the population growth and migration, that the number of patients with malign tissues will rise by 39%, indicating a total number of around 457000 in 2030.<sup>10</sup> This research also pointed out that, not only now but also in the future, the risk of developing cancer will increase with the age of population.<sup>10</sup> Following these results, the previously mentioned types of cancer that mainly occur in one gender will also increase further. In general, the prevalence for every type of cancer will increase in the next 12 years.<sup>10</sup>

Incidence and prevalence may be important for a population, but the total number of deaths and the death rate plays also a key role in cancer statistics. Regarding children, the mortality rises as they grow older. The major part of the children die from tumours of the central nervous system followed by leukemia.<sup>11</sup>

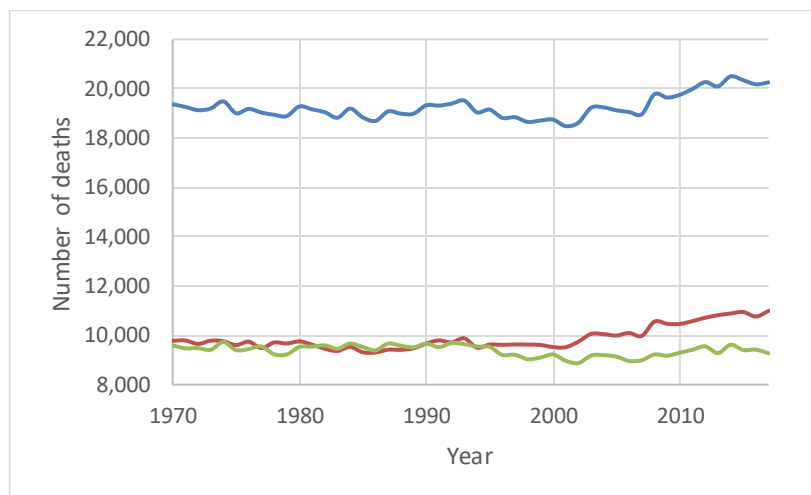


Figure 3: Number of deaths by malignant cancer tissues; the red graph shows the men, the green graph shows the women, the blue graph shows the total amount of victims<sup>1,7</sup>

Figure 3 shows the gender specific, as well as the total number of people, who died over the last 48 years because of cancer. In general, it shows that the mortality will further increase. One positive fact worth noting is that the incidence for certain types of cancer decreases and will further diminish until the year 2030, according to analysis performed by Statistik Austria.<sup>7</sup> Among these are gastric tumours, as well as colon, breast and kidney tumours and those of the female reproductive system.<sup>7</sup>

Moreover, with today's various treatment possibilities the survival of patients diagnosed with cancer will grow. However, the survival rate, of course, decreases the longer the individual is affected by cancer. There is one difference between men and women, when it comes to

surviving cancer: Women have slightly higher chances to live longer with cancer, according to statistics.<sup>12,13,14</sup> It is also obvious that the further a malign tissue has evolved, the less probable it is to survive. For localised tumours the rate of survival is at 87%, whereas only 9% of people with disseminated malign tissues survived in 2012.<sup>13</sup> As already mentioned, it is also important to consider the age of the patients. For children between 0 to 14 years old, the overall survival rate was at 84%, the same is true for teenagers up to 19 years old.<sup>15</sup> For adult people a negative trend is noticed with increasing age. According to data, the chances to survive cancer within 5 years stays the same until the age of 44, then these numbers drop down to 45% for people older than 75 (data shown in Figure 4).<sup>13</sup>

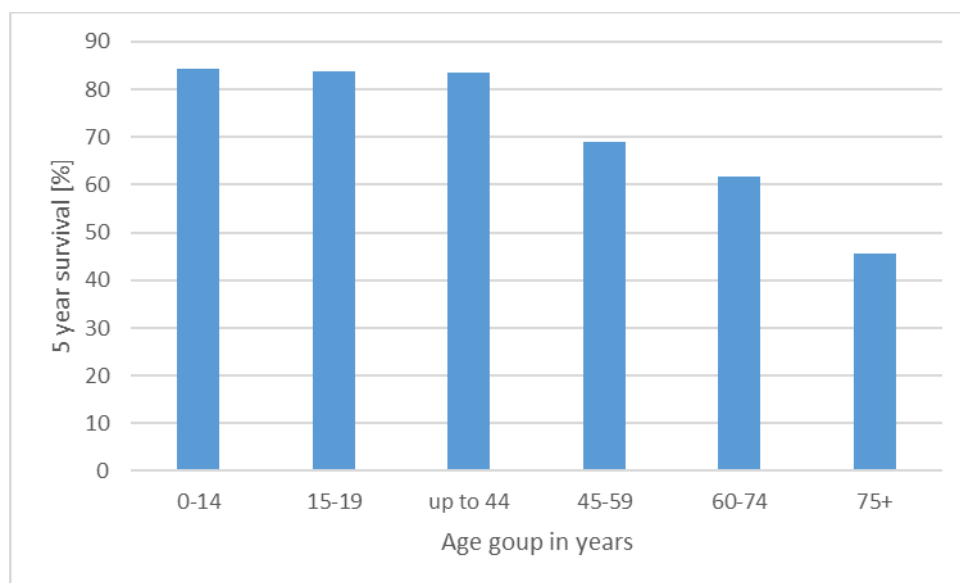


Figure 4: Relative 5 year survival rate of cancer according to the age.<sup>13,15</sup>

In summary, the incidence and prevalence of cancer differs by the type and, therefore, by the affected organ.<sup>2,9</sup> In general, the trend shows an increase in most types of malign tissues, regarding the incidence<sup>2,7</sup> as well as the prevalence,<sup>8,10</sup> but there are also exceptions, which tend to decrease in the near future.<sup>7,10</sup> The overall survival rates increased during the last decades,<sup>13,14</sup> even though it drastically decreases with increasing age.<sup>13,15</sup> Despite the progress in treatment of certain types of cancer,<sup>7</sup> cancer remains a serious issue for our modern society, since a quarter of all deaths are caused by this disease,<sup>16</sup> as illustrated in Figure 5.

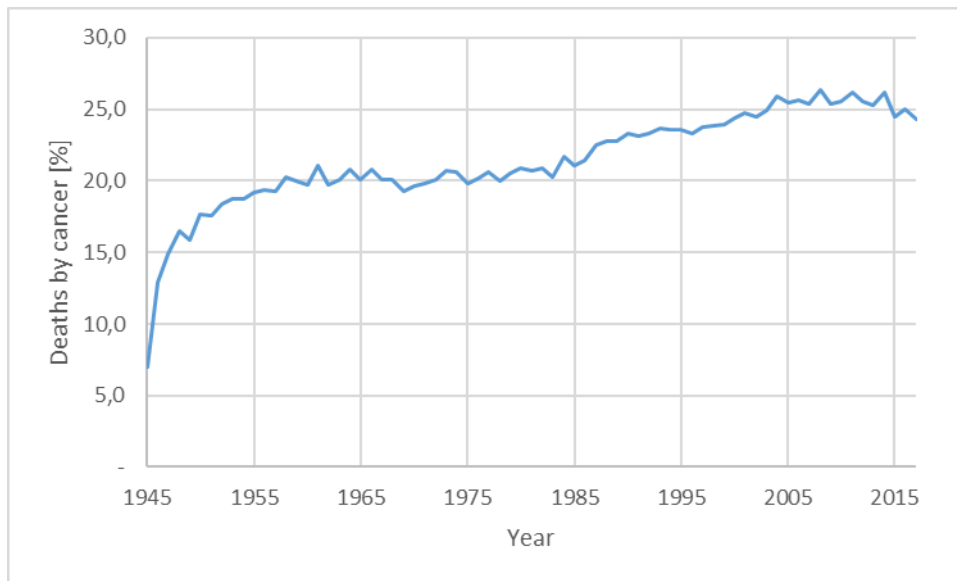


Figure 5: Rate of deaths caused by cancer from 1945 to 2018<sup>16</sup>

## 1.2. Early cancer research

The complex mechanisms of cancer development were originally described by Otto Warburg.<sup>17</sup> His findings published in “On the Origin of Cancer Cells” led to the foundation for today’s understanding of cancer. Warburg concentrated on the energies gained by fermentation and respiration. Both metabolisms have in common that adenosine triphosphate (ATP) is produced, which is rich in energy enabling and sustaining life.<sup>17</sup> The main difference between normal and carcinogenic cells seems to be the amounts of energy gained by the two different types of metabolism. While normal cells produce much more energy by respiration, the amount in cancer cells is approximately the same for both respiration and fermentation. These two processes can easily be distinguished. Respiration is measured in cells, which are saturated with oxygen, by the total consumption of this gas, while fermentation is measured in the absence of oxygen by the formation of lactic acid.<sup>17</sup> Thus, it is obvious that cancer cells are affected by an injury of respiration. Furthermore, the damage of respiration must be irreversible, but, although damage has been inflicted to the respiratory system of the cells, this damage must not be severe enough to kill the cells. If oxygen is drained from normal cells for some hours the major part of them dies because of a lack of energy. Therefore, oxygen is an important tool for the preservation of the viability of normal cells.<sup>17</sup> The increase in fermentation is a result of several distinct impacts. Each impact will be addressed, explaining the latency period of cancer. The cells, which did not increase the fermentation process enough, will not be able to proliferate. Furthermore, it was detected

that fermentation also takes place during the embryonal development and is decreased stepwise.<sup>17</sup>

Even in the 1970's, it was believed that one of the main properties required for cells to be identified as malign was the ability to invade other tissues and metastasise.<sup>18</sup> As Warburg showed in 1956,<sup>17</sup> it is also a common feature for every kind of malign cells to reveal morphological and metabolic changes, most often interpreted as dedifferentiation.<sup>18</sup> During the clonal evolution, the cells are driven towards maximum efficiency concerning proliferation and invasive growth supported by products aiding in this process, like the angiogenesis factor. Two major biological events were recognised at that time:<sup>18</sup>

- The effects of acquired genetic instability
- The sequential selection of variant subpopulations

However, the second event results from the first one. These neoplastic cells also show a higher accumulation of mitotic errors as well as diverse genetic changes. One can suggest that the increase in mitotic events will lead directly to a higher number of errors but, additionally, each single cell division bears a higher risk of genetic alterations.<sup>18</sup> This early research has also shown a correlation between increasing aneuploidy and malignancy.<sup>18</sup> In addition, new approaches also emerged concerning tumour progression, as it may present new surface antigens, which can be interpreted as an epigenetic alteration rather than inherited. To support this theory one has to look at the rates of somatic mutations in normal cells, which are exceeded in malign tissues by far.<sup>18</sup>

Since the human genome was first fully characterised only in 2003<sup>19</sup> the cytogenetics in 1976 remained weak regarding the exploration of genetic phenomena.<sup>18</sup> Despite this lack of understanding of the human genome, it was obvious that certain alterations stimulated the tumour growth, but tumours in different tissues show diverse karyotypes, which lead to the conclusion that for dissimilar environments different changes in the genome might be advantageous.<sup>18</sup>

### 1.3. Status quo of cancer research

Warburg's findings were summarised and extended leading to the conclusion that cancer acquires six vital abilities that govern its malignant growth:<sup>20,21</sup>

- I. Independence from growth signals
- II. Insensitivity to antigrowth signals
- III. Evasion of apoptosis
- IV. Unlimited replicative potential
- V. Sustained angiogenesis
- VI. Tissue invasion/metastasis

All these abilities are acquired during the proliferation of the malignant cells.<sup>20,22</sup> In addition, these unique features grant in some cases malign tissues resistance against drugs.<sup>23</sup>

#### I. Independence from growth signals

Normal cells depend on mitogenic growth signals to move into a proliferating state.<sup>20,22</sup> Those signals are brought into the cell by cell-membrane transmitters. These transmitters bind specific signalling molecules, i.e. diffusible growth factors, cell-to-cell adhesion/interaction molecules and extracellular matrix components.<sup>20,22,24</sup> Normal cells cannot survive without these signals. Many oncogenes found in the cancer catalogue are able to mimic growth signalling pathways.<sup>20</sup>

Research has shown that tumour cells do not mainly depend on exogenous growth stimuli. Thus, those cells may somehow generate their own stimuli to reduce the dependence on the normal cell environment. This leads to a disruption of crucial homeostatic mechanism, which ensures a normal behaviour for non-malignant cells.<sup>20</sup> To achieve this autonomy three strategies on molecular basis have been diagnosed:<sup>20</sup>

- Change in extracellular growth signals
- Change in intracellular circuits translating these signals
- Change in transcellular transducers

In healthy tissues, most soluble growth factors are formed by one specific cell type, whereas cancer cells rely mainly on heterotypic signalling. Every malign cell is able to produce growth signals on its own. Additionally, cancer cells are prone to the growth factors synthesised by themselves. Thus, a positive feedback signalling loop is created, often called autocrine stimulation.<sup>20,24,25</sup>

Cell surface receptors themselves are targets for the deregulation during the pathogenesis of tumours. Malign cells often overexpress growth-factor receptors carrying a tyrosine kinase activity, which enables them to act hyperresponsive to levels of signalling molecules that would not trigger proliferation in normal cells.<sup>20,22,24</sup> Moreover, a vast overexpression of growth-factor-receptors may enable ligand-independent signalling,<sup>26</sup> which can also be achieved by structural changes in the receptors.<sup>20,24</sup> This alteration of receptors is also an essential strategy for cancer cells to achieve resistance against drugs. An example is the enzyme topoisomerase II. While drugs targeting this molecule stabilise the DNA-enzyme complex, cell lines became resistant by a simple mutation in the gene transcribing the topoisomerase II.<sup>23</sup> It is also proven that cancer cells have the ability to switch the integrins, extracellular matrix receptors,<sup>27</sup> to the ones favouring the transmission of pro-growth signals.<sup>24</sup> The impacts of these changes affect the behaviour in terms of enhancing the cell motility in normal tissues, gaining resistance to apoptosis or even the entering in the active cell cycle. Consequently, a failure of these matrix receptors will lead to impairment of cell motility, apoptosis and arresting the cell cycle.<sup>27</sup>

## II. Insensitivity to antigrowth signals

Normal cells receive during their lifespan signals from antiproliferative molecules. These signals are required to maintain the normal behaviour of the cells, including tissue homeostasis and cellular quiescence. Some of these inhibitors are soluble, others are embedded and immobilised on the extracellular matrix or on nearby cells' surfaces. The signals received are conducted by transmembrane cell surface receptors.<sup>20,24</sup>

Those antigrowth signals can counteract proliferation in two different ways: Forcing the cell into the quiescent state out of the proliferation cycle or the complete relinquishment of the proliferation by entering a postmitotic state, which is generally associated with characteristics associated to differentiation.<sup>20</sup> For cancer, two types of signals are important, namely tumour suppressor signals, that must be inactivated to allow growth, and oncogenes, which need to be activated in order to promote progression.<sup>24,28</sup>

Early cancer cells must avoid these antiproliferative signals. Cells usually monitor their environment, whether to proliferate or become quiescent. This quiescence is modulated by the retinoblastoma protein (pRb). It blocks proliferation in hypophosphorylated states by altering certain transcription factors essential for the progression from G1 into S state.<sup>20,24</sup>

With the disruption of the pRb pathway the cell is able to proliferate in succession to the insensitivity to antigrowth factors. This disruption can occur in different ways, e.g. as a downregulation of receptors or as mutated, dysfunctional receptors. The dysfunction may also lead to an elimination, like it is observed in some virus-induced tumours. Moreover, cancer cells have the ability to purposefully silence the expression of extracellular matrix components to favour the ones transmitting pro-growth signals.<sup>20</sup>

Due to the possible change in the matrix components of the cell's membrane, another mechanism to gain resistance emerged. The number of ATP-binding-cassette transporters is increased during the transformation to a malignant cell. These receptors are vital for the efflux of molecules to the extracellular matrix, thus, preventing the cell to accumulate toxins. Since these receptors show high affinities to a large variety of molecules, even to xenobiotics, cells may become resistant to chemotherapeutics.<sup>23</sup>

### III. Evasion of apoptosis

For the transformation of malignant cells into a tumour it is not enough to show immunity against antigrowth signals or to be self-sufficient in pro-growth signals. Another crucial ability of cancer is the evasion of the programmed cell death – apoptosis.<sup>20,22,29</sup>

Nearly every normal cell contains this mechanism and once it is triggered the fragmentation of the cell is completed in up to 2 hours. The complete “dissolution” of the cell fragments may last 24 hours. This mechanism is divided into two different classes, namely the extrinsic/death receptor and the intrinsic/mitochondrial pathways.<sup>20,29,30</sup> Sometimes they are also referred to as sensors and receptors. The sensors fulfil the function of monitoring the extracellular as well as the intracellular environment of cells. Upon scanning signals whether the cell should live or die they

regulate the effectors that induce the apoptotic machinery. These sentinels consist of receptors binding to death or survival factors.<sup>20</sup>

Intercellular sensors observe the cells' condition and induce the apoptotic pathway depending on abnormalities detected. Since most cells receive growth signals via cell-to-cell or cell-to-matrix mechanisms, the vanishing of this communication initiates apoptosis.<sup>20</sup> The ultimate effectors inducing apoptosis include intracellular proteases, named caspases.<sup>20,22</sup> Two so called "gate keeper" caspases (8 & 9) are activated by these death receptors and trigger a cascade of events to activate various other caspases executing the death machinery.<sup>20,29,31</sup> This program can be triggered by an overexpression of an oncogene being activated on a cell surface. Resistance to the apoptotic machinery is acquired by alteration in various ways. One of the most occurring aberrations is observed in the p53 gene.<sup>20,24,29</sup> This gene is found to be corrupted in more than half human malign tissues, involving the elimination of a vital component regarding the DNA damage sensor that is able to trigger the apoptotic cascade. Nearly all malign tissues are expected to obtain alterations enabling the cell to evade the programmed cell death,<sup>20,22</sup> sometimes being followed by resistance to certain drugs.<sup>23</sup> Another important protein family is the BCL-2 family. Upon aberrant expression, the pro-survival factors are overexpressed, which may lead to insensitivity against radiation or chemotherapeutics and other apoptosis inducing agents.<sup>23,29</sup>

#### IV. Unlimited replicative potential

To gain the unlimited potential to replicate, the three previous hallmark capabilities (*vide supra*) need to be acquired. As a result, the program for proliferation is disrupted leading to the growth of tumours. Nevertheless, this is not enough for a tumour to grow expansively. Thus, another independently working mechanism must be apparent to limit the expansion.<sup>20</sup>

As normal cells have a finite potential regarding the replication cycles (Hayflick Limit)<sup>24,32</sup> due to various effects like telomere shortening,<sup>22,24,33</sup> it seems obvious that after a certain number of divisions populations stop growing (for normal cells 60-70), which is called senescence.<sup>20,22,24</sup> To overcome this obstacle, cancer is able to silence two major tumour suppressing proteins and their genes: pRb and p53. The malign tissue will grow as long as a second obstacle appears, which is indicated by cell death,

chromosomal end-to-end fusion<sup>20,22</sup> and the appearance of few single cells being able to proliferate endlessly, thus, being immortal.<sup>20</sup>

This immortalisation is a key component for malign cells to grow and form a tumour. The limitation in cell division is governed by the continuous shortening of the telomers in addition to the inability of DNA polymerases to renew them. Taking this into account the replicative limit for normal cells is a huge barrier for the evolution of macroscopic malignancies. This immortalisation is achieved, to some extent, by an enzyme called telomerase.<sup>20,22,24,33</sup>

It is evident that up to 90% of all tumour tissues show an elevated expression in this enzyme.<sup>20,22,24,33</sup> The remaining cancerous cells show inter-chromosomal changes of telomeric sequences to maintain the length of their telomers, also called ALT (Alternative Lengthening of Telomers) mechanism.<sup>24</sup> These mechanisms are suppressed in normal tissues.<sup>20,34</sup>

Furthermore, telomer lengthening is not the only mechanism responding to DNA damages, since cancer can also gain resistance against the effects of cisplatin. This repairing mechanism leads to resistance by homologous recombination and nucleotide removal repair. Thus, to successfully damage DNA a failure in DNA damage responses in cancer cells is required.<sup>23</sup>

#### V. Sustained Angiogenesis

To be constantly supplied with enough nutrients, cells need to be close, at a maximum of 100 µm, to vessels, especially during the growth of tissues. The process connecting the parenchyma and the vessels is called angiogenesis and is regulated carefully. For a malign tissue it is vital to develop the ability to perform angiogenesis.<sup>20,22,24,35</sup>

Angiogenesis is a process tightly regulated by positive and negative signals, which can be defined as the “angiogenetic switch”. Receptors for pro-angiogenetic signals, as well as their counterparts, are often found on the endothelial cells’ surface. The initiating signals are termed vascular endothelial growth factors (VEGFs) and bind to tyrosine kinase receptors on the cell.<sup>20,22,24</sup>

To maintain this signalling pathway integrins are required. Different integrins are produced from sprouting vessels and quiescent ones. Angiogenesis is not a phenomenon first detected in tumours but is activated earlier as mid-stage lesions

appear. Thus, angiogenesis is an early to mid-stage event in growing malign tissues.<sup>20,22</sup> Another fact being noteworthy is that, without neovascularisation, it is impossible for a tumour to expand massively. This is achieved by unbalancing the “angiogenic switch”,<sup>20,22</sup> since tumours are often able to alter the transcription of genes, leading to an overexpression of VEGFs, for instance, or an increased production of proteases to alter the availability of inhibitors and activators, regarding angiogenesis.<sup>20</sup> Since this neovascularisation needs to be performed at a rapid rate, mistakes in the new blood vessels and the environment are observed. The vessels are leaky and the lymphatic drainage does not work properly. Due to the leakiness in the supplying system, macromolecular molecules may extravasate into malign tissues but not into normal ones. Since the drainage does not work like in normal tissues, incorporated drugs will not be rejected but retained in the tissue. This is called the “EPR-effect” (enhanced permeability and retention) and is a characteristic of the angiogenic growth of tumours.<sup>36–38</sup>

#### VI. Tissue invasion/metastasis

Metastases are described as cells spreading across the body, invading other tissues and grow there independently.<sup>20,22,39</sup> Metastases are responsible for most deaths of cancer patients.<sup>22,24</sup> The invasion of faraway tissues provides new space for the tumour to harvest the nutrients. Furthermore, this new colony does not have limitations in space, regarding its size. To successfully invade other tissues, all of the previously mentioned hallmarks need to be acquired.<sup>20</sup>

Several alterations in the proteins, especially in integrins and cell adhesion molecules, are required to successfully invade or metastasise.<sup>20,24</sup> One example is E-cadherin, which performs an anti-growth effect when bridging adjacent cells. Most epithelial cancers have lost this function. On the other side, overexpression of this molecule leads to impairment of both metastasising and invading tissues.<sup>20,23</sup>

Another way to increase the invasive potential is by a change in extracellular proteases. In this case, the genes possessing protease translation function are upregulated, whereas those genes translating inhibitors of proteases are downregulated. The effect of this alteration is that, when active proteases dock onto the receptors, invasion into the nearby stroma is facilitated, as well as invasion through blood vessels and epithelial

cells. Those proteases do not only play a vital role in invasion and metastasising but also in angiogenesis, as well as in the independency of growth signals.<sup>20</sup> Moreover, research has shown that stromal cells may influence the acquisition of drug resistances. This could be a reason why certain drugs perform well *in vitro* but do not show any potency *in vivo*.<sup>23</sup>

Nevertheless, these hallmark abilities must derive from some earlier occurring events. Hanahan and Weinberg call these features “Enabling Characteristics”.<sup>20,21</sup> They show four independent mechanisms that will affect the probability of being deployed with cancer:<sup>21</sup>

- a) Genomic instability
- b) Inflammation leading to tumour promotion
- c) A reprogrammed energy metabolism
- d) The evasion of destruction by the immune system

a) Genomic instability

Research has shown that all of these “Hallmarks” are results of certain genes being mutated before. These alterations concern the genes of the “caretaker” systems, like DNA repairing proteins or other sentinels monitoring the checkpoints of the cell cycle.<sup>20,40</sup> Although these monitoring systems work efficiently, it is evident that cancer continues to appear in the society, suggesting that mistakes occur.<sup>21</sup> Chromosome/genetic instability involves the rearrangement or even the loss of chromosomes during mitosis favouring, in consequence, genetic adaptations concerning cytotoxic drugs or stressful environments.<sup>40</sup> The role of genomic instability is intensively discussed, since some researchers state that it is acquired in early stages of cancer progression, leading to inactivation or loss of tumour suppressing genes, while others claim it to be a side effect, which facilitates the gain of mutations that eventually confer drug-resistant or aggressive tumours. Since these instabilities are often observed with increased invasiveness, enhanced progression and resistance to drugs, they are mostly observed in metastatic and aggressive tumours.<sup>40</sup> One prominent example for this corruption is the previously mentioned p53 gene, which is mutated in nearly all types of human cancer. Furthermore, an increasing number of corrupted DNA repairing genes

and “cell cycle sentinel” genes is found in certain types of cancer. A partial loss of function or even a general loss allows the growth of malignant cells with diverse properties as mentioned above, due to gene variability and gene instability.<sup>20,21,40,41</sup> Moreover, this genetic instability may lead to an increase in the mutation rate as a result of rising sensitivity to agents with mutating traits governing the way to cells with more aberrant genes.<sup>21</sup>

b) Inflammation leading to tumour promotion

Every newly growing tumour contains cells of the immune system creating minor to huge inflammations. Inflammation of these cells would eventually lead to the destruction of the aberrant tissue. But, in contrast, the inflammation enhances tumour growth and tumorigenesis.<sup>21,24</sup> As a consequence, these immune cells play a vital role for a tumour in the acquisition of hallmarks. They contribute to key bioactive molecules, e.g. survival factors or pro-angiogenetic factors.<sup>21</sup>

c) A Reprogrammed Energy Metabolism

Normal cells live under aerobic conditions. With the provision of glucose, they produce energy (ATP) and carbon dioxide.<sup>42,43</sup> In anaerobic conditions, fermentation plays a vital role, since it is independent from oxygen.<sup>21,43</sup> Cancer has the unique capability to conduct “aerobic glycolysis”. That means that even under aerobic conditions fermentation is favoured to cell respiration. This was discovered by Warburg in 1950.<sup>17</sup> It is commonly known that glycolysis produces much less energy compared to cell respiration.<sup>17,21,44</sup> The reason for malign cells to maintain this form of energy production is the further use of intermediates deriving from this catabolic pathway. This facilitates the biosynthesis of crucial elements for the progression and growth of cancer. This form of metabolism is called “Warburg-like”.<sup>21,22,24,44</sup>

Moreover, some tumours consist of two types of cells differing in their energy metabolism. One uses the Warburg-like pathway (called Warburg effect) by using glucose and secreting lactate,<sup>21,22,45</sup> the other population uses the intermediates provided by the first one, using them as their source of energy. These cells live in symbiosis and this behaviour is not only observed in tumours but also in muscles. The phenotype of fermentation is widespread in malign cells and is just another alteration

induced by oncogenes.<sup>21,45</sup> Following these alterations in metabolic behaviour, cancer cells are able to gain resistance, since many drugs need to be activated through metabolic events. One example for this phenomenon is the expression of metallothionein against platinum based drugs.<sup>23</sup>

d) The evasion of destruction by the immune system

It is still not completely elucidated in how far the immune system plays a role in eradication of a tumorous tissue. Cancer cells are able to circumvent the detection of the immune system or may be able to restrict the immune system, but it is evident that there is a significant barrier to be broken before the tumour can progress.<sup>21,22,24,46</sup> The immune system can attack highly immunogenic cancer cells that are able to provoke immune response by different proteins on the cell surface, also referred to as immunoediting,<sup>22,24,47</sup> leaving only weakly immunogenic cells behind. These variants may be able to form solid tumours. Highly immunogenic tumour cells may survive by disabling some components of the protective system.<sup>21,22,47</sup>

In addition to resistances, if a malign tissue is treated by drugs, it may not be fully eradicated. Some of these cells have properties similar to stem cells and are drug resistant. Another small group possesses capabilities leading to drug resistance. Since these cells are no more sensitive to the drugs applied, they cannot be killed, founding a new, resistant tissue, which might spread across the body.<sup>23</sup>

Moreover, resistances cannot fully be ascribed to genetic mutations. Epigenetic changes play also a vital role and include, for example, DNA methylation and histone modification.<sup>23,48</sup> DNA methylation is most often observed in CpG islands, huge repeating cytosine-guanine groups, all over the genome. In cancer, hypermethylation is common on tumour suppressor encoding genes, thus, silencing them, while it is the opposite for oncogene encoding genes.<sup>23,48</sup>

## 2. Cancer treatment

The treatment of cancer covers a broad range of possibilities nowadays. The most prominent treatment is the surgical removal of malign tissues. Radiation therapy is also a well-known method applied.<sup>49,50</sup> A third method is chemotherapy, which is divided in many different therapies. Some of these therapies will be discussed below.

Since cancer is a highly diverse disease,<sup>20-22</sup> it is clear that this variability offers different methods via exploitation of the characteristic features of cancer. One can, for example, use telomerase inhibitors to counteract the prolongation of telomers in cancer,<sup>21,33,34</sup> use alkylating agents to selectively alkylate thiole groups in proteins or nucleotides from the DNA<sup>51,52</sup> or focus on other hallmarks acquired by cancer.<sup>20,21</sup> The disadvantage of treating cancer with alkylating, especially methylating, agents is that they can change the gene expression sequences by methylating DNA, thus, either increase the repair of DNA or enhance the resistance against drugs.<sup>48</sup>

### 2.1. Transition metal complexes and their clinical use

#### 2.1.1. Platinum

The use of metals as carriers for drugs, as well as the use of their own cytotoxicity, was initiated by the discovery of cisplatin, which is still in use today and one of the best-selling anticancer agents, although severe side effects may occur when applied,<sup>53-55</sup> as well as resistances.<sup>23,53,55</sup> Cisplatin's mode of action includes interstrand cross-linking<sup>53-55</sup> by selectively, covalently binding to adenine and guanine bases.<sup>54,55</sup> First, the complex is hydrolysed exchanging the chloride ligands with water molecules.<sup>56</sup> Recent research also enlightened that cisplatin does not bind preferably to DNA strands but to nucleophilic sites, such as thioles, RNA or proteins, which may be another reason why side effects or resistances occur.<sup>55</sup> In order to bypass these side effects, more research was conducted resulting in the second generation of platinum drugs, namely carboplatin and oxaliplatin (Figure 6).<sup>54,55</sup> Carboplatin exploits the same mode of action as cisplatin. Therefore, it is not potent against cancer being resistant to its progenitor.<sup>55</sup> It is less reactive because of the bidentate dicarboxylato ligand,<sup>54</sup> which eventually leads to a reduction of side effects compared to cisplatin.<sup>54,55</sup> Oxaliplatin differs from the two previous ones,<sup>54,55</sup> since cisplatin resistant cancer can be treated with this drug.<sup>55</sup> Additionally, two liposome incorporated forms of cisplatin

(lipoplatin) and oxaliplatin (lipoxal) are currently in clinical trials showing decreased side effects.<sup>54</sup>

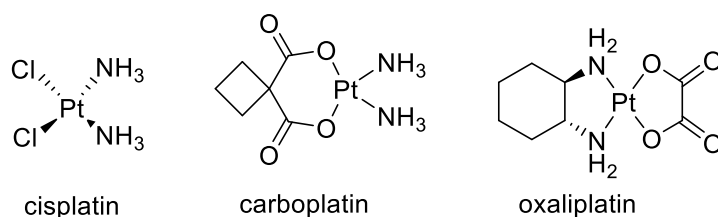


Figure 6: Chemical structures of cisplatin (*cis*-diamminedichloridoplatinum(II)), carboplatin (diammino-cyclobutane-1,1-dicarboxylatoplatinum(II)) and oxaliplatin (1*R*,2*R*-cyclohexane-1,2-diammine-oxalatoplatinum(II)).

Besides the three platinum drugs mentioned, another three platinum(II) complexes are approved for the treatment in humans: lobaplatin, nedaplatin and heptaplatin.<sup>54,55</sup> Nedaplatin shows similar potency to cisplatin.<sup>55</sup> It is approved in Japan.<sup>54,55</sup> Heptaplatin and lobaplatin show similar efficacies to nedaplatin and were approved in South Korea and China, respectively.<sup>54,55</sup> These drugs are shown in Figure 7.

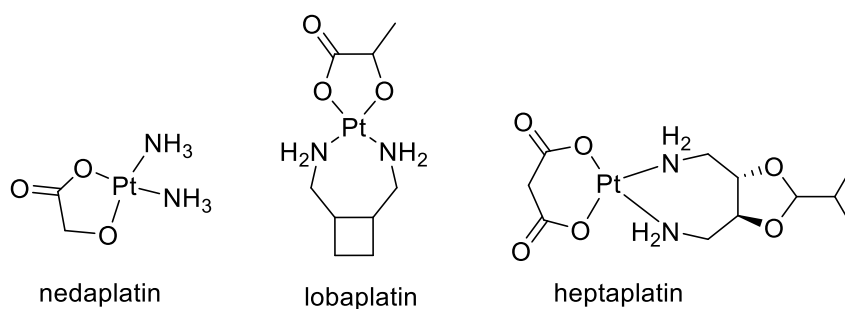


Figure 7: Chemical structures of nedaplatin, lobaplatin and heptaplatin.

All the platinum drugs discussed previously were platinum(II) drugs. To overcome the severe side effects of platinum(II) drugs, novel platinum(IV) drugs like satraplatin or tetraplatin were developed.<sup>57,58</sup> Since the oxidation state is different, platinum(IV) drugs obtain an octahedral coordination sphere allowing to bind two new ligands to the platinum atom, which often have further cytotoxic properties.<sup>57,58</sup> Although the cytotoxicity is generally lower than for platinum(II) compounds, they are more stable in the blood stream<sup>57,58</sup> and can be administered orally.<sup>57,59</sup> Once they are accumulated in the malign tissue, these drugs will there be reduced to platinum(II) releasing the “additional” ligands which can also be biologically active.<sup>57,58</sup> Platinum(IV) complexes being evaluated today in clinical trials are tetraplatin, satraplatin, iproplatin and LA-12.<sup>57</sup> These metal-based drugs are shown in Figure 8.

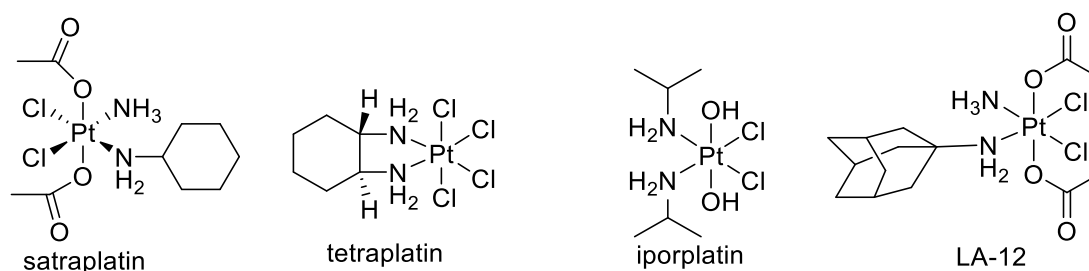


Figure 8: Chemical structures of satraplatin, tetraplatin, iporplatin and LA-12.

### 2.1.2. Ruthenium

Another transition metal which is of interest in cancer treatment is ruthenium, especially in the oxidation states 2+<sup>53-55</sup> and 3+.<sup>53,55</sup> The uptake of ruthenium is thought to be conducted by apotransferrin. This molecule is overexpressed in tumours, since the malign cells require a high amount of iron. Transferrin cannot distinguish between ruthenium and iron, hence, acting as the so-called “Trojan Horse” allowing ruthenium complexes to enter the cell.<sup>60,61</sup> Two different ruthenium(III) prodrugs have entered clinical trials, NAMI-A and KP1019.<sup>55</sup> Although they look structurally similar (see Figure 9), their effects are quite different. NAMI-A is more active against metastases, while KP1019 shows higher efficacy against primary tumours.<sup>53,55</sup>

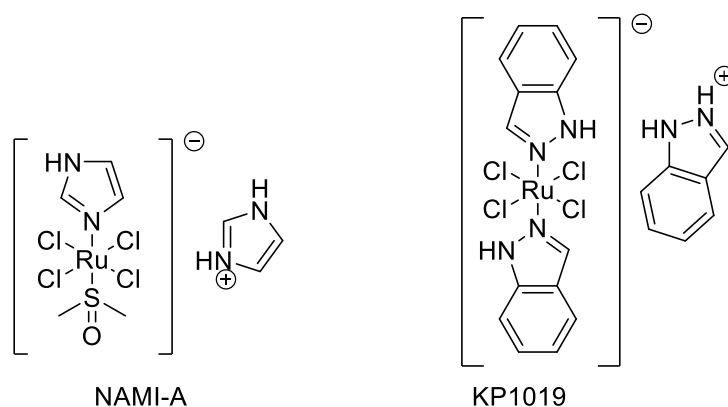


Figure 9: Chemical structures of NAMI-A (1H-imidazolium trans-[tetrachloro-κN-imidazol-κS-dimethylsulfoxideruthenate(III)]) and KP1019 (1H-indazolium trans-[tetrachlorobis(1H-indazole)ruthenate(III)]).

The ruthenium(III) complexes are less active compared to ruthenium(II) congeners. It is supposed that ruthenium(III) complexes undergo activation by reduction to ruthenium(II), but this is not yet confirmed.<sup>53,62</sup> Since this *in vivo* reduction of ruthenium(III) to ruthenium(II) is supposed, the synthesis on ruthenium(II) complexes was stimulated.<sup>53,55</sup> These drugs are mostly half-sandwich/“piano stool” arene complexes including a bidentate ligand and a good leaving group. They show good *in vitro* and *in vivo* activity and their mode of action is different

from that of platinum(II) complexes, although they also bind coordinatively to guanine bases. This might be an explanation for the not occurring cross-resistance.<sup>53</sup> A prominent example is the family of RAPTA complexes.<sup>55</sup> They show high affinity towards cancer cells together with low systemic toxicity. Moreover, their affinity seems to be controlled by pH, since the pH value is lower in cancerous tissues than in normal ones (5.5 and 7.2 respectively). The group of RAPTA complexes (see Figure 10) shows high efficacy against metastases, in contrast to primary tumours, because they effectively trigger cell cycle arrest during the G2/M transition and apoptosis.<sup>55</sup> Ruthenium complexes are not only used as agents targeting DNA strands. Some complexes with enzyme inhibiting properties have been prepared, which show high toxicity against melanoma cells. A ruthenium(II) staurosporine complex acts as an activator for the p53 gene, thus, inducing apoptosis.<sup>53</sup> Recent research shows that the modes of action of ruthenium(II) compounds affect the mitochondrial pathway, ROS mediated apoptosis and the autophagy pathway.<sup>63</sup>

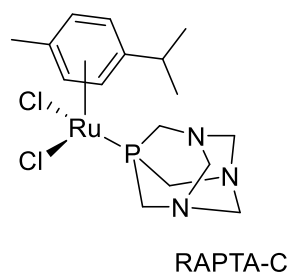


Figure 10: Chemical scaffold of Ru(II) piano-stool complexes represented by RAPTA-C.

### 2.1.3. Copper

Another metal of interest in anticancer research is copper. Its cytotoxic effects are based on the oxidation states copper(I) and copper(II).<sup>55,64</sup> Due to the reversible redox cycling Cu(I)/Cu(II), superoxide radicals, hydroxyl radicals and other reactive oxygen species are generated and DNA might be attacked.<sup>55,64,65</sup> In addition, some copper(II) complexes can induce double strand breaks by intercalating into the DNA or by electrostatic interactions.<sup>55</sup> Copper is an essential trace element, but also reveals general cytotoxicity at high concentrations, damaging the liver, kidneys or the eyes. Copper(II) sulfate, for example, is toxic against liver cells.<sup>64,65</sup> However, an excess of copper(II) is reduced by protection mechanisms, such as those involving metallothioneins, which bind copper(II) and excrete it.<sup>64,65</sup> Moreover, research has shown that copper plays a vital role in angiogenesis.<sup>66</sup> In today's

research, many copper(II) complexes have been synthesised bearing biologically active ligands. One example are quercitine derivatives, which show IC<sub>50</sub> values in a mid to low micromolar concentration range.<sup>64</sup> More recent studies have also provided copper(II) complexes with thiosemicarbazones,<sup>67,68</sup> indoloquinolines<sup>66,69</sup> and Paullones,<sup>70,71</sup> which will be discussed later.

#### 2.1.4. Iron

Iron is another important element for the human body and used as carrier for organic drugs. Cancer needs iron for its growth. Therefore, the transporter protein ferritin is overexpressed on the surface of malign cells<sup>60,72</sup> giving an opportunity for targeted therapy. Iron can also produce reactive oxygen species by reduction of molecular oxygen. It balances the levels of superoxide radical, hydrogenperoxide and hydroxyl radicals, which is also called Fenton-kinetics.<sup>73</sup> Those radicals, especially the highly aggressive hydroxyl radical, are able to damage DNA strands,<sup>73</sup> as already mentioned for copper.<sup>55</sup> Cells rich in free iron may lose their respiratory abilities due to the reactive oxygen species. There are some explanations for mechanisms proposed. First, interaction of lipid components of mitochondrial membranes with these radicals lead to impairment of the respirational activity. Secondly, peroxidation of unsaturated fatty acids generates highly reactive aldehydes, which will, in addition, condense with amino acids, thus, altering enzyme activity. Lastly, a vicious circle will be created, since the binding of iron(II) to membranes will generate oxidative stress and will lead to decreased respiratory activity due to the inactivation of enzymes important for the respiratory chain by functionalising them.<sup>73</sup> Thus, targeted chemotherapy including iron might be a promising approach. The use of iron complexes as chemotherapeutics is well-documented in the literature.<sup>74,75</sup>

There are also other metals currently used in chemotherapy research. Among them titanium,<sup>55</sup> gold,<sup>53</sup> cobalt<sup>53,76</sup> and gallium<sup>53,77</sup> are extensively investigated.

Since the aim of this study lies on the synthesis of indolobenzazepine (IBA) derivatives, the main focus is laid on cyclin-dependant-kinase (CDK) inhibitors and tubulin-polymerase inhibitors, as earlier research has shown that IBAs, with the most prominent molecule class of paullones, exhibit CDK<sup>78,79</sup> as well as tubulin-polymerase inhibition.<sup>80,81</sup>

## 2.2. CDKs and CDK inhibitors

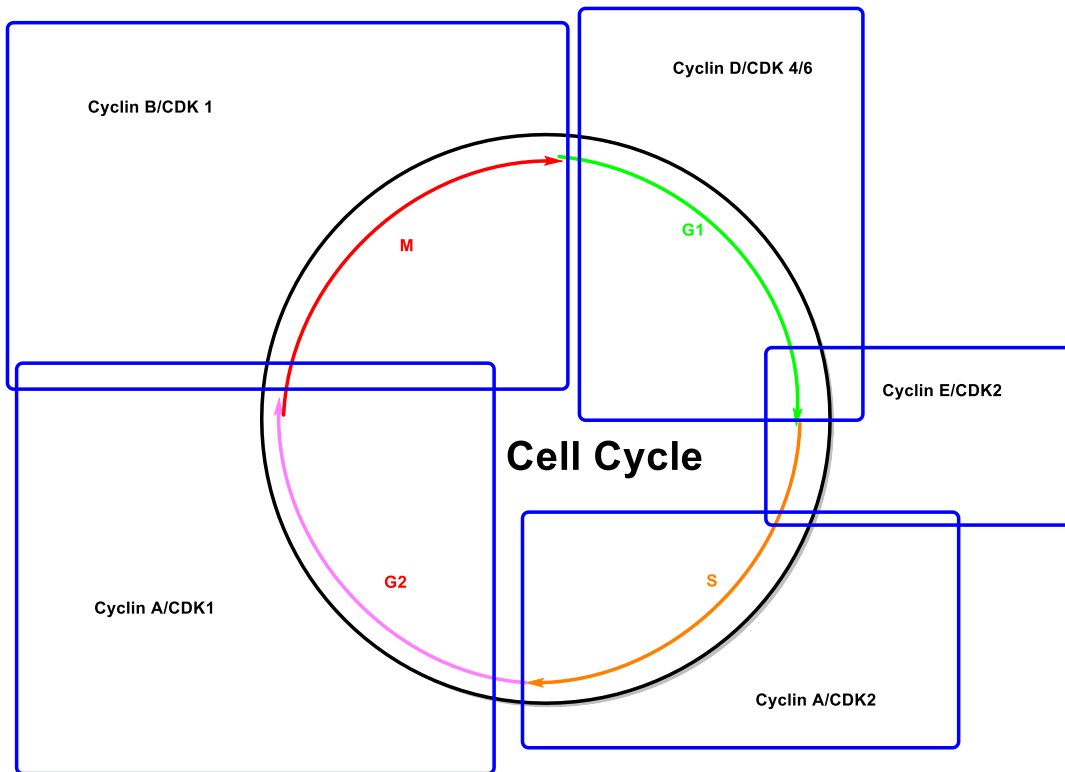


Figure 11: The cell division cycle; the red arrows and labels represent the different phases of the cell cycle; the blue squares show the phases, which are monitored by the corresponding CDK/cyclin complex

As seen in Figure 11, CDKs play a vital role in the cell cycle.<sup>79,82–85</sup> They are so-called checkpoints at each stage of the cycle and are tightly controlled. CDKs are serine/threonine kinases and consist of two different subunits: a catalytic one (the CDK itself) and a regulatory one (the cyclin).<sup>79,82,85,86</sup> Furthermore, each cell-cycle transmission is controlled by a distinct CDK-cyclin complex.<sup>85</sup> The CDKs can be divided into two distinct classes: cell-cycle CDKs and transcriptional CDKs.<sup>82</sup> An important role plays the CDK1 as it has the ability to monitor the progression to the S phase of the cell cycle as well as to control the DNA synthesis. In general, the function is governed by different molecules, they are activated by CDK-activating kinases (CAKs) by positive phosphorylation and inhibited by endogenous inhibitors, short CKIs, through negative phosphorylation.<sup>79,82,84,85</sup> An alteration in the expression of these factors might be associated with hyperproliferation in cancer cells, thus, a dysregulation of this well-balanced system may eventually lead to tumorigenesis.<sup>82,84,85</sup>

In cancerous cells the CDK pathways are disturbed.<sup>79,82–86</sup> The retinoblastoma proteins normally inhibit the transition from the G1 phase into the S phase during the cell cycle but are inactivated by two CDKs, CDK4 and 6.<sup>79,82,85</sup> This alteration is commonly found

in human cancer cell lines, thus, this aberration plays a vital role in tumorigenesis.<sup>82,83,85</sup> On the other hand, if CDK4 is inhibited, the tumour undergoes cell death and regression.<sup>82</sup>

Another important CDK is CDK2. It monitors the so-called restriction point together with cyclin E.<sup>82</sup> The restriction point is the transition from G1 phase to S phase.<sup>82,83,87</sup> An alteration, e.g. an increase in cyclin E levels, will eventually lead to enhanced proliferation.<sup>82,84</sup>

CDK1 is sometimes also called the major regulator of mitosis.<sup>85</sup> Upon the complexation with its own cyclin, it is able to start mitosis. It is supposed that a deregulation in the levels of cyclin B1 may cause cancer. This complex is the sentinel for the transmission from G2 phase to M phase, thus, a watchman for damaged DNA not to be doubled.<sup>82</sup> Therefore, with elevated levels of this sentinel, it is possible to induce the cell-cycle arrest in G2/M transmission, which enables scientists to exploit cell cycle arrest.<sup>82,85</sup>

Apart from CDKs being involved in the cell-cycle, other CDKs are involved in transcriptional regulation.<sup>82</sup> Examples are CDK7, which is an important part of the “general transcription factor II Human”, but also works as a CDK-activating kinase, or CDK8, which regulates a controlling gene-specific transcription and its deficiency probably leads to arrested embryonic development.<sup>82</sup>

CDK5 does not have similar effects but also plays major roles in proliferation, survival and migration of cancer. It is also proposed that it might be important for the cell-cycle in similar ways like CDK2 and 4.<sup>82</sup>

Furthermore, CDKs regulate metabolism, epigenetic regulation or spermatogenesis.<sup>82</sup> Based on these facts, it is not surprising that CDKs are promising targets for anticancer therapy.

CDK inhibitors can be divided in ATP-competitive and ATP-non-competitive.<sup>85</sup> A competitive agent is flavopiridol.<sup>79,82,85,86</sup> It is an alkaloid isolated from plants and was the first CDK inhibitor that underwent clinical trials. Research suggests its capability to inhibit the most forms of CDKs,<sup>82,85,86</sup> thus, it is called a pan-CDK inhibitor.<sup>82,84</sup> It has the ability to inhibit both cell-cycle CDKs by blocking transitions from G1 to S phase and G2 to M phase,<sup>79,82</sup> as well as transcriptional CDKs (7 & 9).<sup>82</sup> Flavopiridol shows effective inhibition in cell tests against CDKs with nanomolar IC<sub>50</sub> values.<sup>79,82,85,86</sup>

Although preclinical trials showed great promise for this alkaloid,<sup>82,85,86</sup> clinical trials were not satisfying, since severe side effects were observed,<sup>82,84-86</sup> e.g. nausea, neutropenia or diarrhoea.<sup>82,85</sup>

After the discovery of the various effects of flavopiridol many different CDK inhibitors were synthesised aiming to reduce unwanted toxicities and improving the selectivity towards CDKs. One example is palbociclib, which is an ATP competitive inhibitor with high selectivity for CDK4 and 6. Today it is used to treat breast cancer.<sup>82-86</sup> Another example is ribociclib, which shows affinity towards CDK4 and 6 as well,<sup>82,83,86</sup> and seliciclib, also known as R-roscovitine.<sup>82,85,86</sup> Although all of these compounds show potent activity against a broad range of tumours,<sup>82,83,85,86</sup> except for R-roscovitine, where only some analogues show activity,<sup>82</sup> they often have mild to severe side effects, e.g. neutropenia for palbociclib and ribociclib.<sup>82,83</sup>

The main strategy to treat cancer patients with CDK inhibitors is combination therapy with other cytotoxic drugs. Since the potency of these CDK inhibitors applied as single agents is moderate, preclinical as well as clinical studies suggest synergistic effects when incorporated with other cytotoxic drugs.<sup>82,83,85</sup> They may arrest the cell cycle, thus, other agents' cytotoxicity will be improved. A prominent example is the combination of ribociclib with an aromatase inhibitor, which has recently gained approval by the FDA as initial therapy against advanced breast cancer. However, the risk of QT-prolongation (the ventricular action potential duration),<sup>88</sup> which may eventually lead to death because of polymorphic ventricular tachycardia,<sup>89</sup> increases as this combination is applied.<sup>82</sup> Another example for combining CDK inhibitors and additional drugs is abemaciclib and fulvestrant. This combination is also approved by the FDA for the treatment of advanced breast cancer.<sup>82</sup> Although these combinations show improvement in cytotoxicity against cancer cells, side effects are still present in most combinations, not only for the ones mentioned.<sup>82,83,85</sup> Some examples of CDK inhibitors in use are shown in Figure 12.

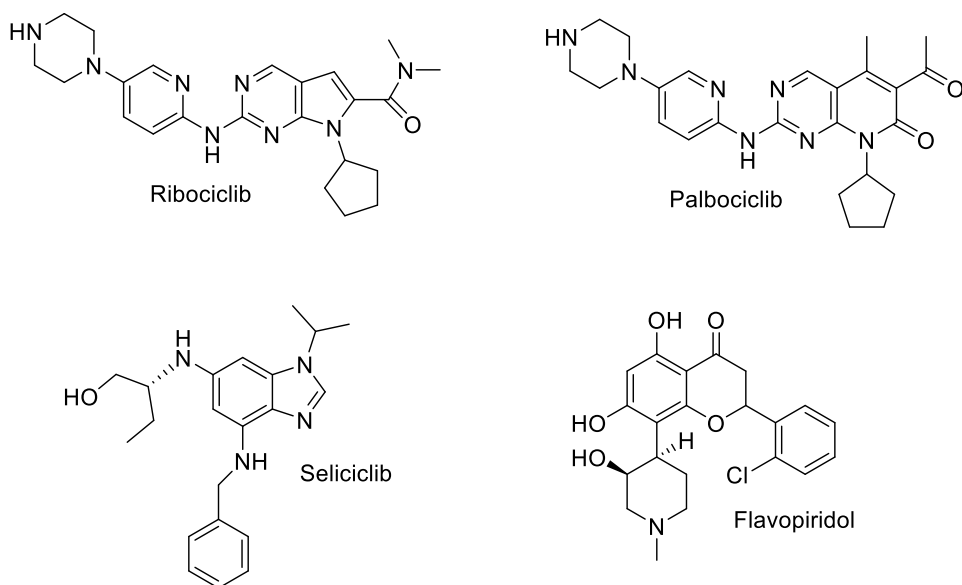


Figure 12: Chemical structures of Ribociclib, Palbociclib, Seliciclib and Flavopiridol

### 2.3. Tubulin and tubulin-inhibitors

The tubulin-inhibitors were first recognised by scientists as possible anticancer agents in 1967, when the mode of action of colchicine was discovered.<sup>90</sup> The mode of action of microtubule targeting agents (MTAs) can be distinguished between two manners: tubulin mass can either be increased/stabilised (microtubule stabilising agents, MSAs) or decreased/destabilised (microtubule destabilising agents, MDAs).<sup>90–93</sup> As a consequence, when these dynamics are disturbed, mitotic block and apoptosis will be triggered,<sup>90,94</sup> since they are able to arrest the cell-cycle in G2/M phase.<sup>91–93</sup> Moreover, this type of anticancer agent can be applied either as single-agent therapy or to a larger extent in combination with other drugs.<sup>94–96</sup>

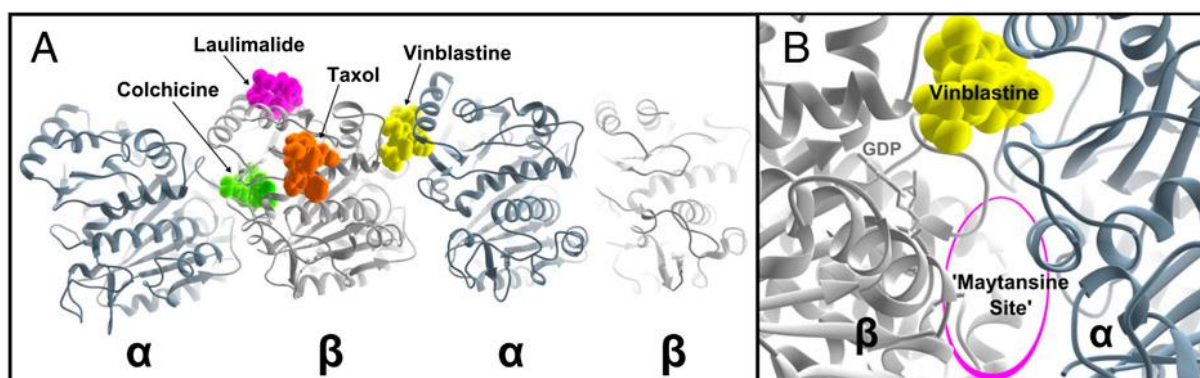


Figure 13: Tubulin subunits with different drug binding sites included. The figure is used with permission from Ref.<sup>97</sup> © Senter P., 2014, Proceedings of the National Academy of Sciences.

The general structure of tubulins is made up of two distinct compartments, the  $\alpha$  and the  $\beta$  subunits. Their functions cover a broad spectrum, e.g. chromosome segregation during mitosis, intracellular transport or cell shape maintenance.<sup>90-92</sup> The two sub-classes of microtubule-inhibitors, MSAs and MDAs, work differently. MSAs act as they bind to yet polymerised tubulin subunits, thus, stabilising them. MDAs, in contrast, bind to the tubulin dimers and destabilise them.<sup>90-93</sup> Many MTAs are derived from naturally occurring molecules, like vinca alkaloids. Up to now, three different binding sites are confirmed, the taxane-, vinca alkaloid- and colchicine binding site.<sup>90-93</sup> Two more have recently been disclosed, laulimalide<sup>90,92,93</sup> and peloruside binding sites.<sup>90</sup> These are shown in Figure 13.

A prominent group of molecules acting as MDAs are vinca alkaloids, like vinblastine, vincristine and vinorelbine<sup>90,93,96</sup> (see Figure 14). These molecules are a subclass of the so-called “Phytochemicals”, which are secondary metabolites of plants.<sup>98</sup> One main application of these natural products is the treatment of breast cancer,<sup>94,98,99</sup> as well as brain cancer.<sup>95</sup> Additionally, their properties include the inhibition of metastases and angiogenesis.<sup>95,98,99</sup> Combination therapies show big advantages regarding single-agent therapy, since they enhance the efficiency of the partner drug, sensitise cancer cells against radiation and, most importantly, in different drug resistant breast cancer cell-lines resistance was circumvented by applying combination therapy including phytochemicals like vinca alkaloids.<sup>98</sup>

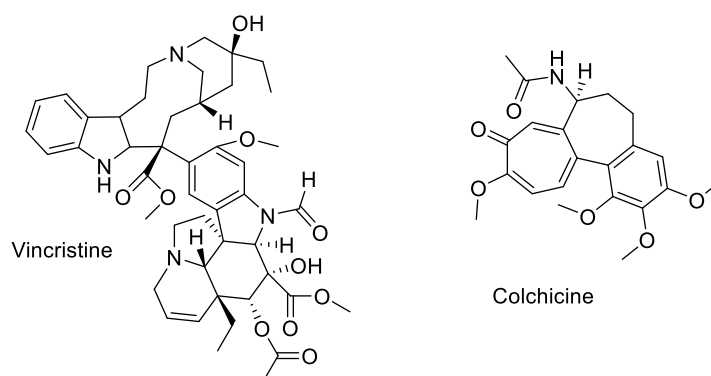


Figure 14: Structure of vinca alkaloids represented by Vincristine and Colchicine.

Many MTAs being synthesised show great activity *in vitro* as well as *in vivo*. Nevertheless, they suffer from big disadvantages, since they are poorly soluble in water, barely bioavailable<sup>90-92</sup> and highly toxic.<sup>90,96</sup> One approach to circumvent these

obstacles may be targeted drug delivery.<sup>90</sup> Moreover, drug-resistance may appear as expression of ATP-binding cassette reporters in tumours.<sup>23,91,92</sup> Research indicates that this problem can be resolved, if colchicine-site binding molecules are used,<sup>91,92</sup> since colchicine showed more promising results in taxane resistant breast cancer cells than vinblastine, an alkaloid.<sup>98</sup> One example is combrestatin A-4 (CA4). It shows potent activity against various cell lines, also including the ones being multidrug-resistant, despite being poorly water-soluble. The increase in activity against cancer cells was achieved when different sodium phosphate salts were synthesised.<sup>91,93</sup>

So far, a plethora of prodrugs has been documented targeting the colchicine binding-site. CA4-analogues have already been mentioned.<sup>90,92,93</sup> Moreover, N-acetylcholchicol prodrugs, as well as a benzophenone prodrug bearing a trimethoxyphenyl unit are under current investigation. Some of them revealed increased aqueous solubility and less toxic effects.<sup>90,92</sup> In addition, molecules binding to the colchicine binding-site have proven to be antiangiogenic and vascular disrupting, thus, preventing tumour growth.<sup>90,93,99</sup> Research has also shown that incorporation of certain moieties bring additional antiproliferative activity, e.g. trimethoxyphenyl or indole.<sup>92</sup> Li et al.<sup>92</sup> reported indoles condensed with TMP-bearing units, which have structural features similar to the desired skeleton described in this thesis (see Figure 15).

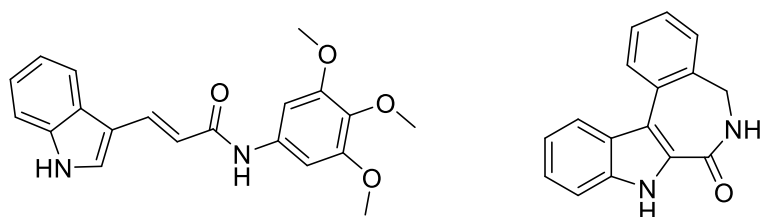


Figure 15: Indole based scaffold presented by Li et al.<sup>92</sup> (left) and the desired scaffold (right).

With the knowledge of the mode of actions of CDK and tubulin, and how to control these proteins, as well as the cancer specific resistances, new anti-tumour agents may now specially be designed and synthesised.

## 2.4. Indolobenzazepines

Up to now, paullones have gained much attention in cancer therapy. Diverse synthetic pathways were proposed for the synthesis of this scaffold and other derivatives.<sup>78,93,100–102</sup>

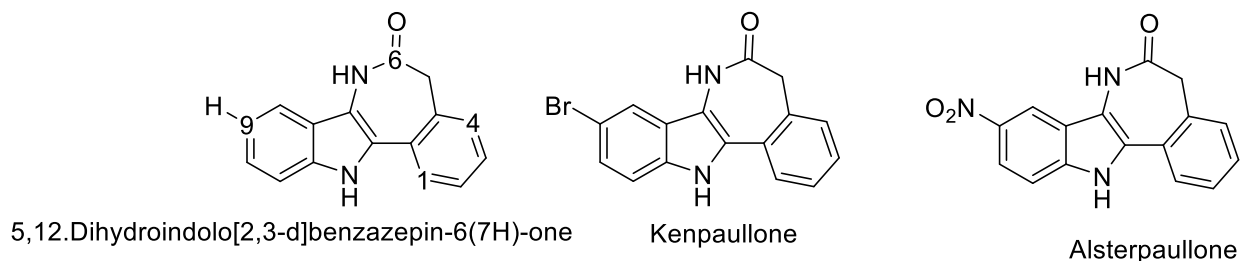
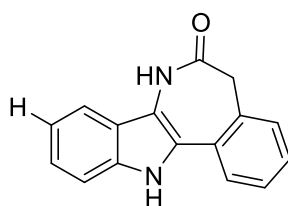


Figure 16: 5,12-Dihydroindolo[2,3-d]benzazepin-6(7H)-one, Kenpaullone and Alsterpaullone in comparison.

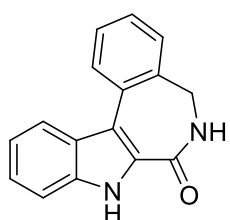
Figure 16 shows three species differing by their substituent in position C9. One of the first synthetic approaches to this compound class was proposed in 1999 by Schultz et al.<sup>103</sup> These authors have prepared derivatives, beginning with a low substituted skeleton, the kenpaullone, and extending it to a more developed one, the 2,3-dimethoxy-9-trifluoromethyl-5,12-dihydroindolo[2,3-d]benzazepine-6(7H)-one.<sup>103</sup> In addition, they evaluated the IC<sub>50</sub> values in a kinase assay for CDK1 with cyclin B and compared these results with traditional CDK-inhibitors, namely flavopiridol (IC<sub>50</sub> = 0.3 μM) and roscovitine (0.65 μM).<sup>103</sup> The results showed that substitution at various positions had marked effects on the inhibition. While the relatively low substituted 2-bromokenpaullone shows equal efficacy to flavopiridol, 4-methoxy-paullone was not efficient at all (IC<sub>50</sub> = 430 μM). On the other hand, alsterpaullone showed improved CDK inhibitory behaviour, since its IC<sub>50</sub> value is about a tenth of flavopiridol (0.035 μM). It seems that the inhibition of CDK1 is favourable with Paullones bearing electron withdrawing substituents in position 9.<sup>103</sup> It should be noted that other functional groups, the lactam unit and the indole nitrogen, were also aims for derivatisations. The results showed that none of the conducted alterations at these specific positions (N<sub>12</sub>, O<sub>6</sub>) showed an increase in inhibitory efficacy but a decrease up to 1 mM for 5,12-bisbutyloxycarbonylkenpaullone, leading to the conclusion that the nitrogen-atoms may play a role in the mode of action.<sup>103</sup> The anti-tumour activity against HCT-116 colon cancer cells revealed that, although drugs with strong inhibition against CDK1 showed high cytotoxicity, the anticancer effect from Paullones may not derive from their ability to inhibit CDK1, since derivatives with very high IC<sub>50</sub> values in the kinase assay showed good antiproliferative potency.<sup>103</sup> Further studies were conducted on kenpaullone to evaluate the efficacy against different kinases, including more CDKs, protein

kinases and casein kinases. Most kinases tested were not inhibited, except the CDKs 1 to 5, where high affinity was observed. Just the switch from kenpaullone to 10-bromopaullone turned the data up-side-down.<sup>104</sup> Most kinases inhibited by kenpaullone were inhibited worse, but, in contrast, kinases not inhibited by kenpaullone were inhibited by its derivative. Zaharevitz et al. concluded that the skeleton of paullones serves as a good template to be altered for further approaches in the synthesis of CDK inhibitors.<sup>104</sup>

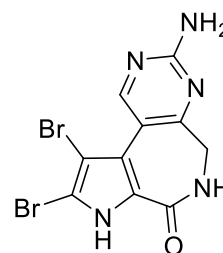
Another class of compounds used in fighting cancer was that of latonduine derivatives. Latonduine A did not show any inhibition against a range of kinases and also no cytotoxicity was observed.<sup>105</sup> Yet, extending the pyrrole unit to an indolo scaffold apparently affects the cytotoxicity and anticancer properties tremendously. French researchers proposed indolobenzazepinones related to the structure of paullones (see Figure 17) that might be able to induce cytotoxicity by disturbing the dynamics of tubulin polymerisation.<sup>80,81,106</sup>



5,12-Dihydroindolo[2,3-d]benzazepin-6(7H)-one



5,8-Dihydroindolo[2,3-d][2]benzazepin-7(6H)-one



Latonduine A

Figure 17: 5,12-Dihydroindolo[2,3-d]benzazepin-6(7H)-one, the desired Indolobenzazepine (5,8-Dihydroindolo[2,3-d][2]benzazepin-7(6H)-one) and Latonduine A in comparison.

Not much research has been done in the field of synthesis of indolobenzazepinones, apart from paullones and related derivatives. Latonduine derivatives are another promising class of potential chemotherapeutics. The French scientists replacing the pyrrole moiety by an indole unit have synthesised a plethora of derivatives, sometimes alkylated,<sup>81,106</sup> or with different ring sizes.<sup>80</sup>

*In vitro* tests against KB cells, oral squamous cancer cells,<sup>107,108</sup> showed that the unsubstituted indolobenzazepine possesses high activity with an IC<sub>50</sub> value of 0.55 μM. Better performance was observed with the racemic C5 methyl substituent, where the cytotoxicity is almost doubled (IC<sub>50</sub> = 0.28 μM). Surprisingly, the racemic mixture displayed an averaged cytotoxicity, since the *R*-isomer was less cytotoxic (IC<sub>50</sub> = 0.34 μM) when compared to the *S*-isomer (IC<sub>50</sub> = 0.08 μM).<sup>106</sup> The ethyl substituted derivative was even more cytotoxic and *R*- and *S*-isomers did not differ so much, with 0.035 and 0.037 μM, respectively. Further lengthening of the group at C5 had no effect on the activity.<sup>106</sup> These IC<sub>50</sub> values are comparable with those of colchicine (IC<sub>50</sub> = 0.02 μM). Nevertheless, the increase in activity by alkylating the C5 carbon is only observed by linear alkyl substituents. Moreover, the lactam moiety plays an important role, as well as the indole nitrogen, since the reduction of the lactam to the amine and methylation of both or only the indole nitrogen resulted in a tremendous loss in activity, with IC<sub>50</sub> values of 12, 28 and 7 μM, respectively.<sup>106</sup> Interestingly, the *S*-ethyl substituted indolobenzazepine showed an activity similar to colchicine in a variety of cancer cell lines, indicating that the activity is independent from the cell line.<sup>106</sup> Since these molecules are proposed to arrest the cell cycle by binding to tubulin, cell cycle progression was monitored upon use of the most cytotoxic indolobenzazepine. It was observed that a variety of cells arrest in the G2/M phase, while some cells of the same cell line arrest at higher doses.<sup>106</sup> Eventually, after 24 h, all cells underwent apoptosis. The effect of the cytotoxicity is well overlapping with their ability to disturb the dynamics of tubulin, which could be observed by the deformation and shrinkage of cells during the deployment. *In vivo* experiments also showed that tumour mass decreased quickly, but not as quickly as when treated with colchicine.<sup>106</sup>

Derivatives with unsubstituted seven- and eight-membered rings showed high cytotoxicity in MCF7 cell lines with IC<sub>50</sub> values of 0.3 and 0.2 μM, respectively. The nine-membered ring-containing species revealed IC<sub>50</sub> values of 8 μM. Further substitution decreased the cytotoxicity tremendously.<sup>80</sup> A broad variety of derivatives was tested for their tubulin disturbing properties. All compounds attacked tubulin partially or completely, inhibiting the assembly of the microtubules with IC<sub>50</sub> values ranging from 3.7 to 15.9 μM. Additionally, all these derivatives showed anti-tumour activities in nanomolar concentration range.<sup>80</sup> The conclusion was drawn that the lower the IC<sub>50</sub> values were, the more competitive the derivative was against colchicine in cell tests. Nevertheless, not every compound showed competition with colchicine for the respective binding site.<sup>80</sup>

One drawback of paullones, even though they possess low micromolar  $IC_{50}$  values, is their low aqueous solubility and bioavailability. As a consequence, peripheral modifications are required to enhance the solubility.<sup>109–111</sup> One approach, which was explored in this work, is the coupling to a morpholine moiety. This moiety was shown to markedly improve the pharmacological profile of different drugs.<sup>112,113</sup>

As to paullones related scaffold, the indoloquinoline, also attracts interest of researchers for the development of anticancer drugs. Indoloquinolines exhibit high antiproliferative potency, often higher than that of related indolobenzazepines. This might be due to their structure, since indoloquinolines are highly conjugated flat systems. Indolobenzazepines have an additional carbon atom in the benzazepine ring, which is  $sp^3$  hybridised, thus, disrupting the aromatic system, resulting in a nonplanar, folded structure (see Figure 18).<sup>69</sup>

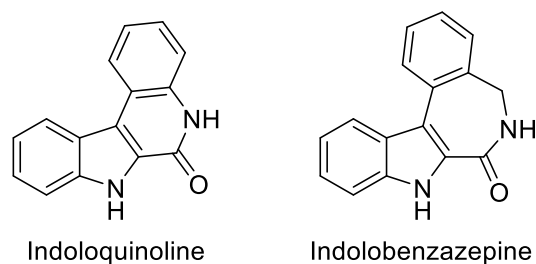


*Figure 18: The indoloquinoline scaffold in contrast to the indolobenzazepine scaffold.*

Indolobenzazepines and related scaffolds show very low  $IC_{50}$  values,<sup>80,106</sup> but improvement needs to be done concerning the solubility in water. This may be achieved by complex formation with transition metals. Different metals are suitable that adopt various coordination numbers and, thus, coordination geometries, accessible redox-states in the window of biologically relevant redox potentials and ligand exchange rates.<sup>53,55</sup>

## 2.5. Metal complexes with paullone derived ligands

The first paullones used for complex formation with transition metals were reported in 2006 by Dobrov and coworkers.<sup>114</sup> This approach led to a series of gallium(III) complexes, as well. The first complexes were synthesised with kenpaullone derivatives,<sup>114</sup> since paullones do not have suitable binding sites for complex formation with metals. The sites being able to bind metals, the lactam or the derivatised thiolactam unit, would only form four-membered metallocycles, which are thermodynamically not stable.<sup>109</sup> The derivatisation of paullones was undertaken to introduce new binding sites being able to accommodate metal ions. The complex formation with metal ions will have a number of positive effects, e.g. stabilisation of unusual or unfavoured ligand geometries, redox activity, enhanced cellular uptake as well as increased aqueous solubility and maybe synergistic biological effects regarding the metal centre and the ligands.<sup>109</sup> The results from the syntheses of the first paullone complexes were encouraging. The complexes as well as the corresponding ligands were tested in different cell lines. The complexes showed enhanced antiproliferative activity cancer cell lines. The enhancement was by a factor from 1.5 to 17.9. Nevertheless, clarity is required whether the cytotoxicity resulted from the independent activity of ligand and central ion, or whether the complex shows an individual mode of action.<sup>114</sup>

Further efforts were focused on the synthesis of complexes of paullones with ruthenium(II)<sup>109,111</sup> and osmium(II).<sup>111</sup> The ruthenium(II) complexes showed IC<sub>50</sub> values comparable to that of kenpaullone.<sup>109</sup> These results show that ruthenium(II) and osmium(II) arene complexes are beneficial to the pharmacological profile of these drugs. This counteracts the results from Schultz et al., since they described kenpaullone as the more potent derivative.<sup>103</sup> The results are even counteracting to such an extent that, for kenpaullone derived complexes, the IC<sub>50</sub> values from two of the three cell lines tested could not be determined, since they were too high. Thus, the conclusion was drawn that the antiproliferative activity might be derived from non-covalent bonding or intercalation with DNA. Regarding the changes occurring in the secondary structure of the DNA, intercalation is the preferred hypothesis.<sup>109</sup> A comparison was also drawn between the osmium(II) arene and ruthenium(II) arene complexes. Again, the IC<sub>50</sub> values ranged in the micromolar to sub-micromolar region for both ruthenium complexes (0.53 to 2.5  $\mu$ M) and osmium complexes (0.63 to 2.2  $\mu$ M). These osmium(II) complexes were among the most active osmium complexes so far. Because of these similarities in antiproliferative activity, the conclusion was

drawn that the mode of action is independent from the metal centre.<sup>111</sup> Quite recently, however, this hypothesis was debated. The results showed that the ruthenium complexes were more active towards cancer cells than osmium complexes, but the IC<sub>50</sub> values are again in the low micromolar to sub-micromolar range.<sup>115</sup> An explanation might be that the ligands used affect the metal centre, hence, leading to different or the same toxicological profiles when applied.

Moreover, not only ruthenium and osmium complexes were synthesised with paullone ligands. Copper complexes were also reported.<sup>66</sup> The cytotoxicity resembles that for the osmium and ruthenium complexes with IC<sub>50</sub> in the low micromolar to sub-micromolar concentration range. In this case, the complexes with derivatised kenpaullone scaffold showed higher potency than complexes with the unsubstituted paullone derivatives. It is outlined that complex formation has strong, positive effects on the solubility and pharmacokinetic behaviour. One complex exhibited the mid to low nanomolar IC<sub>50</sub> values in all cells tested.<sup>66</sup>

These kind of complexes have been further developed, in particular, metal complexes with paullones bearing additional free-radical TEMPO unit were reported. These TEMPO bearing ligands were synthesised with copper,<sup>70</sup> ruthenium and osmium.<sup>71</sup> The osmium and ruthenium complexes showed good antiproliferative activity with IC<sub>50</sub> values in the low micromolar range. It should be noted that the free ligand showed lower IC<sub>50</sub> values (sub-micromolar) than the complexes, but revealed decreased aqueous solubility. In contrast, the ligand without the free radical unit showed markedly decreased antiproliferative activity, suggesting that the free radical plays a vital role in the cytotoxicity of these ligands.<sup>71</sup> The target of these drugs might be the supercoiled DNA. Both ruthenium and osmium complexes affect the secondary structure of the DNA, with ruthenium having slightly stronger effects. They may also form interhelical bridges leading to large DNA conglomerates, thus, being less mobile.<sup>71</sup> The copper(II) complexes also showed highly antiproliferative properties. The IC<sub>50</sub> values were all in the sub-micromolar to nanomolar concentration range. The TEMPO unit enhanced the cytotoxic effect. The complex formation with copper(II) did not result in further increase in the cytotoxicity.<sup>70</sup> However, the complexes showed promising ribonucleotide reductase inhibitory potential, since after half an hour 60% of the tyrosyl-radicals were quenched and upon addition of dithiothreitol the tyrosil radicals completely disappeared after 20 seconds.<sup>70</sup>

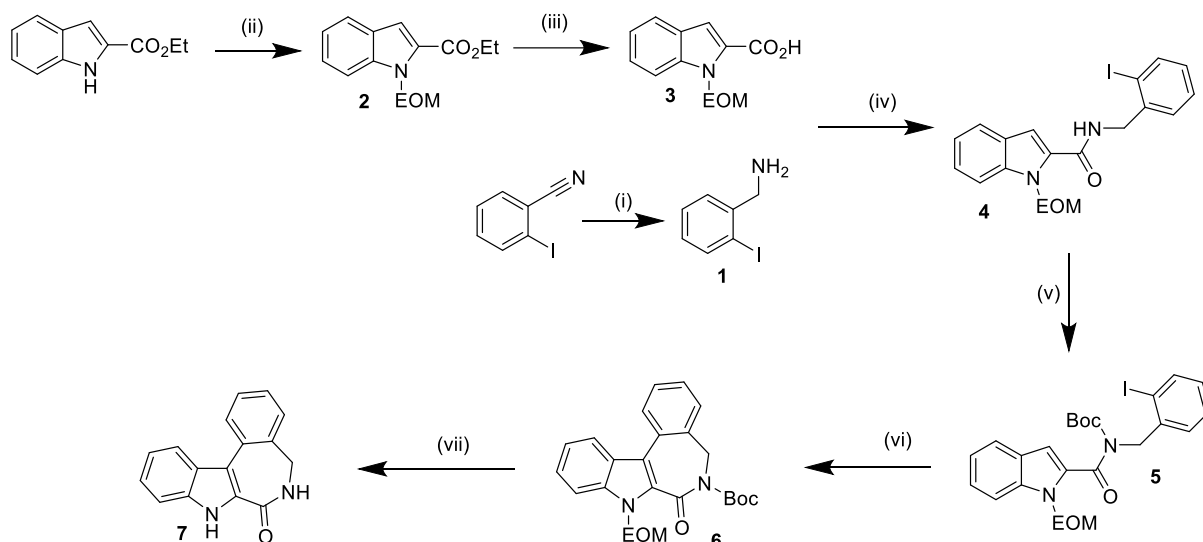
In general, the IC<sub>50</sub> values of the complexes mentioned are strongly cell line dependent.

### 3. Experimental part

2-Iodobenzonitrile and ethyl-1*H*-indole-carboxylate were purchased from ABCR. The BH<sub>3</sub> (1M in THF), absolute DMF, dimethylaminopyridine, di-*tert*-butyl-dicarbonate, absolute acetonitrile, palladium(II) acetate, sodium bicarbonate, basic aluminum oxide and 2-picolinaldehyde were bought from Acros Organics. Ethoxy-methylchloride was obtained from TCI. Sodium hydride, phosphorus(V) sulfide, celite, hydrazine monohydrate and methyl iodide were bought from Sigma Aldrich, while lithium hydroxide monohydrate and triphenylphosphine from Alfa Aesar. Magnesium sulfate was bought from Fisher Chemicals. 1-Ethyl-3-(3-dimethylaminopropyl)carbodiimide-hydrochloride was ordered from IRIS biotech. Silver(I) carbonate was bought from Merck.

#### 3.1. Synthesis of 5,8-dihydroindolo[2,3-*d*][2]benzazepin-7(6*H*)-one

The synthesis of indolobenzazepine was performed by following the procedure reported by Putey et al.,<sup>105</sup> as shown in Scheme 1.



Scheme 1: Synthesis pathway to achieve the underivatized indolobenzazepine;  
(i): Argon, THF, 0°C, 80°C; (ii): Argon, DMF, 0°C, RT; (iii): Ethanol, LiOH·H<sub>2</sub>O, reflux; (iv): Argon, DCM, 0 °C, RT; (v): Argon, MeCN, RT; (vi): Argon, DMF, 100 °C; (vii): Dioxane, 1N HCl, reflux

### **2-Iodobenzylamine (1)**

Under argon-flush 2-Iodobenzonitrile (6 g, 26.22 mmol) was dissolved in absolute THF, which was then cooled to 0°C. The borane-complex (1M in THF, 60 mL) was added dropwise, then the solution was refluxed for 2 hours. After cooling it again to 0 °C, ethanol (24 mL) was added dropwise, then 1N HCl in methanol (36 mL) was added dropwise. The solvent was removed under reduced pressure and the oily residue was taken up in saturated potassium carbonate solution (90mL) and extracted with dichloromethane (3 × 100 mL). The organic phases were dried over magnesium sulfate and concentrated *in vacuo*. The raw product was purified on silica using a mixture of dichloromethane : methanol : trimethylamine 95 : 4 : 1 as eluent. The product was obtained after evaporation of the solvent as a yellow oil. Yield: 5.1 g, 83%. <sup>1</sup>H NMR (500 MHz, DMSO-*d*<sub>6</sub>) δ 7.80 (dd, *J* = 7.8, 1.1 Hz, 1H), 7.52 – 7.48 (m, 1H), 7.38 (td, *J* = 7.5, 1.1 Hz, 1H), 6.98 (td, *J* = 7.8, 1.7 Hz, 1H), 3.66 (s, 2H), 1.89 (ddd, *J* = 91.0, 52.5, 20.7 Hz, 2H).

### **Ethyl-1-(ethoxymethyl)-1*H*-indole-2-carboxylate (2)**

Under argon-flush ethyl 1*H*-indole-2-carboxylate (6 g, 31.8 mmol) was dissolved in absolute DMF (60 mL). The solution was cooled to 0 °C and sodium hydride (60 % in mineral oil, 1.91 g, 47.7 mmol) was added carefully, as the reaction is highly exothermic and hydrogen is formed. The reaction mixture was stirred at room temperature for 1 h before it was again cooled to 0 °C. Then ethoxy-methylchloride (5.91 mL, 63.6 mmol) was added dropwise and the mixture was stirred at room temperature overnight. The solvent was removed under reduced pressure and the residue taken up in water (40 mL). The aqueous solution was extracted with dichloromethane (4 × 40 mL). The combined organic phases were dried over magnesium sulfate and concentrated *in vacuo*. The raw product was purified on silica using a mixture of hexane : ethylacetate 95 : 5 as eluent. The product was isolated as a white solid after evaporation of the solvent. Yield: 8 g, 99%. <sup>1</sup>H NMR (500 MHz, DMSO-*d*<sub>6</sub>) δ 7.71 (dd, *J* = 12.2, 8.3 Hz, 2H), 7.40 – 7.35 (m, 2H), 7.21 – 7.16 (m, 1H), 5.98 (s, 2H), 4.34 (q, *J* = 7.1 Hz, 2H), 3.42 – 3.36 (m, 2H), 1.34 (t, *J* = 7.1 Hz, 3H), 1.02 (t, *J* = 7.0 Hz, 3H).

### **1-(ethoxymethyl)-1*H*-indole-2-carboxylic acid (3)**

Ethyl-1-(ethoxymethyl)-1*H*-indole-2-carboxylate (**2**) (6.45 g, 26.1 mmol) was dissolved in ethanol (75 mL). To this solution a solution of LiOH·H<sub>2</sub>O (1.31 g, 31.3 mmol) in water (10 mL) was added and the reaction mixture was refluxed for 2 h. Then the solvent was evaporated to give an oil. This oil was dissolved in water (70 mL) and acidified with 1N HCl (45 mL). The white, voluminous precipitate was extracted with dichloromethane (4 × 60 mL). The combined organic phases were dried over magnesium sulfate and concentrated *in vacuo*. The crude product was recrystallised from 1 : 1 hexane : ethylacetate as eluent, resulting in white needles. Yield: 5.4 g, 94%. <sup>1</sup>H NMR (500 MHz, DMSO-*d*<sub>6</sub>) δ 13.03 (s, 1H), 7.72 – 7.63 (m, 2H), 7.36 (ddd, *J* = 8.3, 7.0, 1.1 Hz, 1H), 7.30 (d, *J* = 0.6 Hz, 1H), 7.20 – 7.14 (m, 1H), 6.00 (s, 2H), 3.44 – 3.36 (m, 2H, overlapped with residual water), 1.02 (t, *J* = 7.0 Hz, 3H).

### **1-(ethoxymethyl)-*N*-(2-iodobenzyl)-1*H*-indole-2-carboxamide (4)**

Under argon-flush 2-Iodobenzylamine (**1**) (3.45 g, 14.8 mmol) was dissolved in dry DCM (150 mL). The solution was cooled to 0 °C and 1-(ethoxymethyl)-1*H*-indole-2-carboxylic acid (**3**) (2.95 g, 13.5 mmol), 1-Ethyl-3-(3-dimethylaminopropyl)carbodiimide-hydrochloride (2.84 g, 14.8 mmol) and dimethylaminopyridine (1.65 g, 13.5 mmol) were added. This solution was stirred in the ice bath overnight and at room temperature for more 2 days. Then water (40 mL) was added and the solution was acidified with 6N HCl to pH ≈ 1. After the separation of the phases the mixture was extracted with dichloromethane (3 × 40 mL). The combined organic phases were dried over magnesium sulfate and concentrated *in vacuo*. The crude product was washed with ice cold ether affording a white solid. Yield: 6.67 g, 99%. <sup>1</sup>H NMR (500 MHz, DMSO) δ 9.18 (t, *J* = 5.8 Hz, 1H), 7.89 (d, *J* = 7.7 Hz, 1H), 7.69 (d, *J* = 7.9 Hz, 1H), 7.65 (d, *J* = 8.4 Hz, 1H), 7.39 (t, *J* = 7.4 Hz, 1H), 7.31 (t, *J* = 7.3 Hz, 2H), 7.26 (s, 1H), 7.16 (t, *J* = 7.4 Hz, 1H), 7.05 (t, *J* = 7.0 Hz, 1H), 5.97 (s, 2H), 4.41 (d, *J* = 5.8 Hz, 2H), 3.41 – 3.36 (m, 2H, overlapped with residual water signal), 1.00 (t, *J* = 7.0 Hz, 3H).

### **Tert-butyl (1-(ethoxymethyl)-1*H*-indole-2-carbonyl)(2-iodobenzyl)carbamate (5)**

Under argon flush 1-(ethoxymethyl)-*N*-(2-iodobenzyl)-1*H*-indole-2-carboxamide (**4**) (13.72 g, 31.6 mmol) was dissolved in acetonitrile (500 mL). Di-*tert*-butyl-dicarbonate (11.03 g, 50.5 mmol) and a catalytic amount of dimethylaminopyridine were added. The yellow solution was stirred overnight and turned orange. The solvent was evaporated and the residue was taken up in water (100 mL). It was partitioned with ethylacetate (2 × 100 mL). Afterwards it was dried over magnesium sulfate and concentrated *in vacuo*. The raw product was purified on silica using a mixture of hexane : ethylacetate 85 : 15 as eluent. The product was obtained as a white solid after evaporation of the solvent. Yield: 14.26 g, 85%. <sup>1</sup>H NMR (500 MHz, DMSO-*d*<sub>6</sub>) δ 7.91 (dd, *J* = 7.8, 1.0 Hz, 1H), 7.72 – 7.67 (m, 2H), 7.43 (td, *J* = 7.6, 1.0 Hz, 1H), 7.35 (ddd, *J* = 8.3, 7.1, 1.0 Hz, 1H), 7.26 – 7.22 (m, 1H), 7.17 (dd, *J* = 11.1, 4.1 Hz, 1H), 7.08 – 7.04 (m, 2H), 5.76 (s, 2H), 4.87 (s, 2H), 3.44 (q, *J* = 7.0 Hz, 2H), 1.10 (s, 9H), 1.07 (t, *J* = 7.0 Hz, 3H).

### **6-*Tert*-butyl 8-(ethoxymethyl)-5-dihydroindolo[2,3-*d*][2]benzazepin-7-one (6)**

Under argon flush *tert*-butyl (1-(ethoxymethyl)-1*H*-indole-2-carbonyl)(2-iodobenzyl)carbamate (**5**) (6.19 g, 11.57 mmol) was dissolved in absolute DMF. Palladium(II) acetate (130 mg 0.58 mmol), triphenylphosphine (304 mg, 1.16 mmol) and silver(I) carbonate (6.40 g, 23.14 mmol) were added and stirred at 100°C for 1 h. The DMF was removed *in vacuo* and the black residue taken up in dichloromethane (50 mL). It was filtered over celite and rinsed with dichloromethane (50 mL). The raw product was purified on silica using a mixture of hexane : ethylacetate 85 : 15 as eluent. The product was obtained as a white solid after evaporation of the solvent. Yield: 4,62 g, 98%. <sup>1</sup>H NMR (500 MHz, DMSO-*d*<sub>6</sub>) δ 8.05 (dd, *J* = 7.9, 3.9 Hz, 2H), 7.83 (d, *J* = 8.5 Hz, 1H), 7.62 – 7.54 (m, 2H), 7.52 – 7.43 (m, 2H), 7.32 (t, *J* = 7.6 Hz, 1H), 6.05 (d, *J* = 10.8 Hz, 1H), 5.92 (d, *J* = 10.8 Hz, 1H), 5.09 (d, *J* = 15.0 Hz, 1H), 4.26 (d, *J* = 14.9 Hz, 1H, overlapping with residual water), 1.47 (s, 9H), 1.03 (t, *J* = 7.0 Hz, 3H).

### 5,8-dihydroindolo[2,3-*d*][2]benzazepin-7(6*H*)-one (7)

6-Tert-butyl 8-(ethoxymethyl)-5-dihydroindolo[2,3-*d*][2]benzazepin-7-one (**6**) (5.2 g, 12.79 mmol) was dissolved in dioxane (250 mL). 1N HCl (100 mL) was added and the resulting mixture was heated to 80°C for 2 h while stirring. The solution was neutralised with sodium bicarbonate and then extracted with dichloromethane (3 × 200 mL). The organic phases were afterwards dried over magnesium sulfate. The solvent was removed under reduced pressure and the raw product was purified on silica using a mixture of dichloromethane : methanol 99 : 1 as eluent. The product was obtained as a white solid after recrystallisation in methanol. Yield: 2.46 g, 78%. <sup>1</sup>H NMR (500 MHz, DMSO-*d*<sub>6</sub>) δ 12.04 (s, 1H), 8.41 (t, *J* = 5.4 Hz, 1H), 8.01 (d, *J* = 8.1 Hz, 1H), 7.95 (d, *J* = 7.5 Hz, 1H), 7.55 (d, *J* = 8.2 Hz, 1H), 7.49 (dd, *J* = 14.7, 7.2 Hz, 2H), 7.34 (ddd, *J* = 8.1, 6.0, 2.5 Hz, 2H), 7.20 (t, *J* = 7.6 Hz, 1H), 4.07 (d, *J* = 5.2 Hz, 2H).

### 3.2. Synthesis of proligands

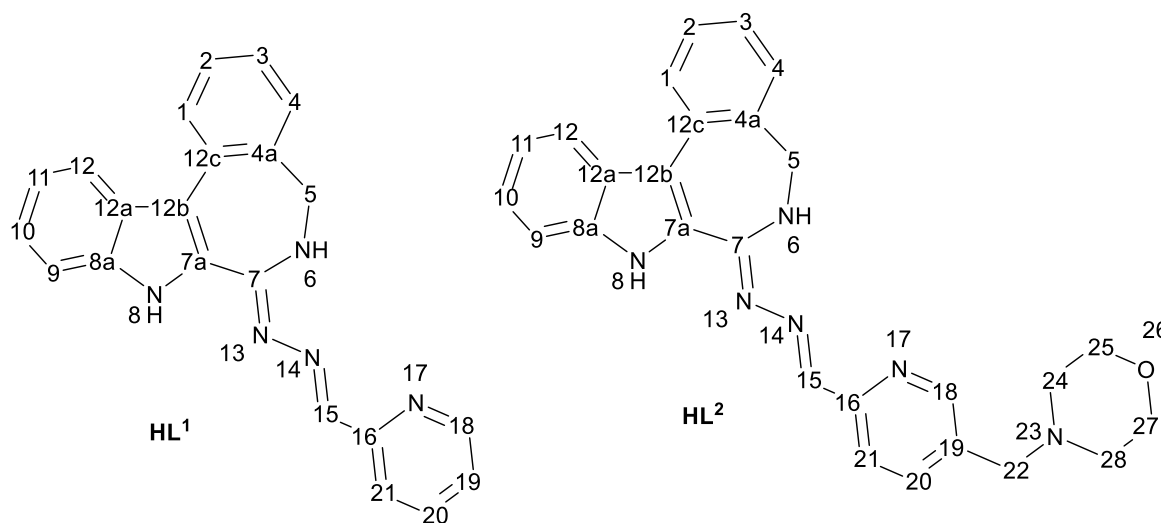
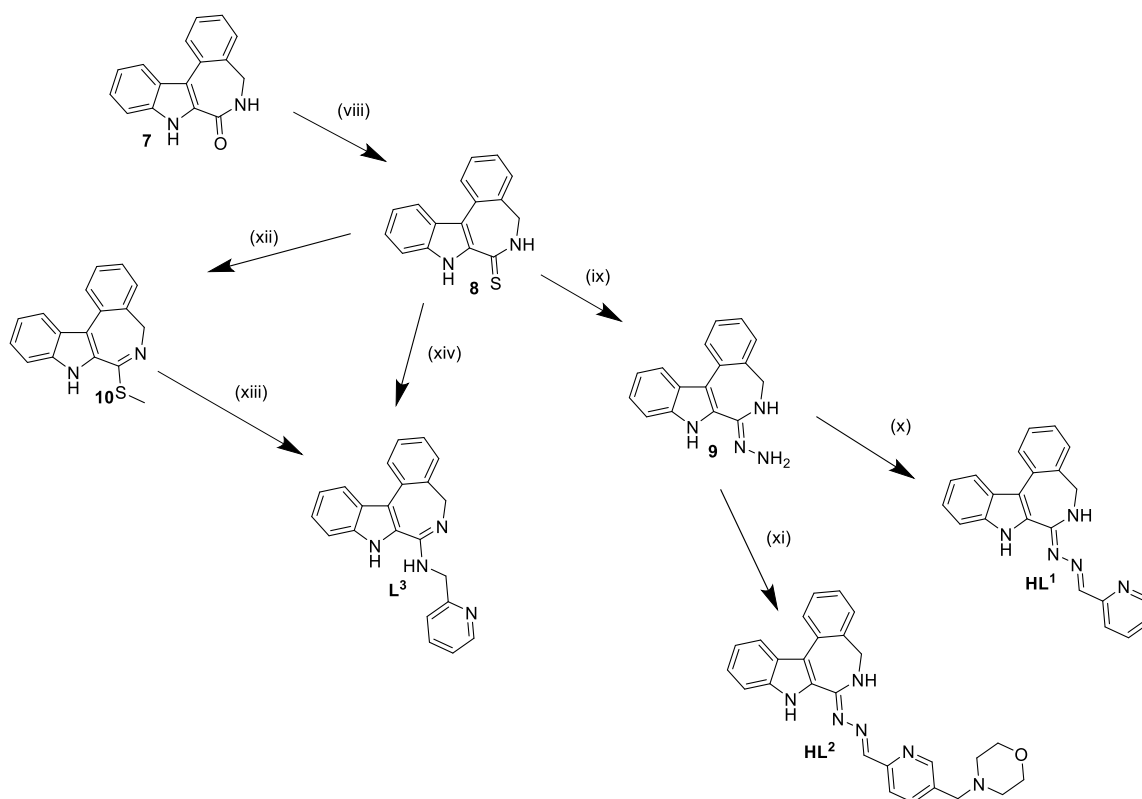


Figure 19: Ligands desired including the NMR numbering scheme.

For the synthesis of the different ligands protocols were followed, which were primarily used for paullones by Primik et al.<sup>66</sup> and Schmid et al.<sup>110</sup> The synthetic pathway is shown in Scheme 2. Thionation of the main scaffold was conducted as reported by Polshettiwar and Kaushik.<sup>116</sup>



Scheme 2: Synthesis pathway of the three desired ligands;  
 (viii): Argon, MeCN, Al<sub>2</sub>O<sub>3</sub>·P<sub>4</sub>S<sub>10</sub>, reflux; (ix): H<sub>2</sub>N-NH<sub>2</sub>·H<sub>2</sub>O, 135°C, (x): Argon, Ethanol, Picolinaldehyde, 95°C; (xi): Argon, Ethanol, 5-(morpholinomethyl)picolinaldehyde; 90°C; (xii): Argon, NaH, THF, MeI, reflux; (xiii) and (xiv) showed no conversions

### 5,8-dihydroindolo[2,3-*d*][2]benzazepin-7(6*H*)-thione (**8**)

Under argon flush 5,8-dihydroindolo[2,3-*d*][2]benzazepin-7(6*H*)-one (**7**) (966 mg, 3.9 mmol) was dissolved in absolute acetonitrile (7.7 mL) in a Schlenk tube. Argon was bubbled through the solution for 15 min after adding Al<sub>2</sub>O<sub>3</sub>·P<sub>4</sub>O<sub>10</sub> (1.6 g, 0.34 equiv P<sub>4</sub>O<sub>10</sub>). The reaction was stirred at 90 °C overnight with the Schlenk tube covered in tin foil. The suspension was filtered and the residue was washed with acetonitrile. The filtrate was concentrated *in vacuo*, taken up in water (50 mL) and brought to pH ≈ 8 with saturated potassium carbonate solution. The solution was extracted with dichloromethane (3 × 100 mL). The organic phases were combined and dried over magnesium sulfate. The dried organic phase was concentrated and the raw product was purified on silica using a mixture of dichloromethane : methanol 99 : 1 as eluent. The product crystallised as yellow needles in small amounts of methanol. Yield: 841 mg, 82%. <sup>1</sup>H NMR (500 MHz, DMSO-*d*<sub>6</sub>) δ 11.85 (s, 1H), 10.64 (s, 1H), 8.05 (dd, *J* = 14.2, 8.0 Hz, 2H), 7.70 (d, *J* = 8.3 Hz, 1H), 7.59 (dd, *J* = 10.6, 4.4 Hz, 1H), 7.55 (d, *J* = 6.5 Hz, 1H), 7.50 – 7.46 (m, 1H), 7.42 (dd, *J* = 11.2, 4.0 Hz, 1H), 7.27 (t, *J* = 7.5 Hz, 1H), 4.40 (s, 1H), 4.13 (s, 1H). ESI-MS (acetonitrile/methanol + 1% water). positive: 265.08 [(**8**) + H]<sup>+</sup>

### 7-hydrazineyl-5,8-dihydroindolo[2,3-*d*][2]benzazepin(6*H*) (9)

5,8-dihydroindolo[2,3-*d*][2]benzazepin-7(6*H*)-thione (8) (582 mg, 2.21 mmol) was dispersed in hydrazine-mono hydrate (8 mL) under argon atmosphere. The solution was heated to 135 °C and stirred overnight. After cooling the suspension was allowed to stand in the fridge for 4 h. Then the light yellow product was filtered off and dried *in vacuo*. Yield: 496 mg, 86%. <sup>1</sup>H NMR (500 MHz, DMSO-*d*<sub>6</sub>) δ 11.43 (s, 1H), 7.86 (t, *J* = 8.5 Hz, 2H), 7.49 – 7.40 (m, 2H), 7.37 (d, *J* = 6.5 Hz, 1H), 7.20 (dt, *J* = 21.5, 7.3 Hz, 2H), 7.09 (t, *J* = 7.0 Hz, 1H), 6.32 (s, 1H), 5.00 (s, 2H), 4.07 (s, 2H). ESI-MS (acetonitrile/methanol + 1% water). positive: 263.12 [(9) + H]<sup>+</sup>.

### (E)-7-(2-(pyridin-2-ylmethylene)hydrazineyl)-5,8-dihydroindolo[2,3-*d*][2]benzazepin(6*H*)one (HL<sup>1</sup>)

In an argon-flushed Schlenk flask 7-hydrazineyl-5,8-dihydroindolo[2,3-*d*][2]benzazepin(6*H*) (9) (199 mg, 0.76 mmol) was suspended in ethanol (3 mL). After 10 min of bubbling argon through the solution, picolinaldehyde (79.4 μL, 0.83 mmol) was added. The mixture was stirred at 95 °C overnight. The product was precipitated with water. Afterwards ethanol (10 mL) was added until the solution became clear. The solution was concentrated slowly *in vacuo*, but not to dryness. The yellow precipitate was filtered off, washed with water and dried *in vacuo*. Yield: 266 mg, 99%. Anal. Calcd for C<sub>22</sub>H<sub>17</sub>N<sub>5</sub>·0.4C<sub>2</sub>H<sub>6</sub>O (M = 372.13 g mol<sup>-1</sup>): C, 73.71; H, 5.07, N, 19.09. Found: C, 73.91; H, 5.33; N, 18.82. <sup>1</sup>H NMR (500 MHz, DMSO-*d*<sub>6</sub>) δ 11.93 (s, 1H, H<sup>12</sup>), 8.59 (d, *J* = 4.1 Hz, 1H, H<sup>18</sup>), 8.37 (d, *J* = 8.0 Hz, 2H, H<sup>15</sup>, H<sup>21</sup>), 8.31 (t, *J* = 5.4 Hz, 1H, H<sup>6</sup>), 7.98 (dd, *J* = 15.4, 7.6 Hz, 2H, H<sup>12</sup>, H<sup>3</sup>), 7.87 (td, *J* = 7.5, 1.2 Hz, 1H, H<sup>20</sup>), 7.60 (d, *J* = 8.2 Hz, 1H, H<sup>9</sup>), 7.53 – 7.49 (m, 1H, H<sup>2</sup>), 7.47 (d, *J* = 6.6 Hz, 1H, H<sup>4</sup>), 7.40 – 7.31 (m, 3H, H<sup>10</sup>, H<sup>1</sup>, H<sup>19</sup>), 7.20 (dd, *J* = 11.1, 4.0 Hz, 1H, H<sup>11</sup>), 4.36 – 4.02 (m, 2H, H<sup>5</sup>). <sup>13</sup>C NMR (151 MHz, DMSO) δ 155.62 (Cq, C<sup>7</sup>), 154.52 (Cq, C<sup>16</sup>), 152.14 (CH, C<sup>15</sup>), 149.28 (CH, C<sup>18</sup>), 137.78 (Cq, C<sup>4a</sup>), 136.76 (Cq, C<sup>8a</sup>), 136.30 (CH, C<sup>20</sup>), 133.161 (Cq, C<sup>12c</sup>), 129.01 (Cq, C<sup>7a</sup>), 128.09 (CH, C<sup>4</sup>), 128.06 (CH, C<sup>2</sup>), 127.41 (CH, C<sup>3</sup>), 126.33 (CH, C<sup>1</sup>), 124.94 (Cq, C<sup>12a</sup>), 124.10 (CH, C<sup>10</sup>), 123.87 (CH, C<sup>19</sup>), 120.77 (CH, C<sup>21</sup>), 120.46 (CH, C<sup>11</sup>), 120.22 (CH, C<sup>12</sup>), 117.12 (Cq, C<sup>12b</sup>), 112.69 (CH, C<sup>9</sup>), 46.00 (CH<sup>2</sup>, C<sup>5</sup>). ESI-MS (acetonitrile/methanol + 1% water). positive: 352.26 [HL<sup>1</sup> + H]<sup>+</sup>, 725.27 [(HL<sup>2</sup>)<sub>2</sub> + Na]<sup>+</sup>.

**(E)-4-((6-((2-(5,8-dihydroindolo[2,3-*d*][2]benzazepin-7(6*H*)-yl)hydrazineylidene)methyl)pyridin-3-yl)methyl)morpholine (HL<sup>2</sup>)**

Under argon flush 7-hydrazineyl-5,8-dihydroindolo[2,3-*d*][2]benzazepin(6*H*) (**9**) (241 mg, 0.92 mmol) was suspended in ethanol (3 mL). Argon was bubbled for 10 min through the solution. Then 5-(morpholinomethyl)picolinaldehyde (209 mg, 1.01 mmol) was added. The solution was stirred at 90 °C overnight. The product was precipitated with water. Ethanol (10 mL) was added to the suspension to dissolve the precipitate. The solution was concentrated *in vacuo*, but not to dryness. The product was isolated by filtration and dried *in vacuo* to give a yellow powder. Afterwards the product was dried *in vacuo*. Yield: 398 mg, 98%. Anal. Calcd for C<sub>27</sub>H<sub>26</sub>N<sub>6</sub>O·1.1H<sub>2</sub>O (M = 470.35 g mol<sup>-1</sup>): C, 68.93; H, 6.07, N, 17.81. Found: C, 68.94; H, 6.04; N, 17.87. <sup>1</sup>H NMR (600 MHz, DMSO-*d*<sub>6</sub>) δ 11.92 (s, 1H, H<sup>8</sup>), 8.50 (d, *J* = 1.4 Hz, 1H, H<sup>18</sup>), 8.36 (s, 1H, H<sup>15</sup>), 8.32 (d, *J* = 8.1 Hz, 1H, H<sup>21</sup>), 8.27 (t, *J* = 5.3 Hz, 1H, H<sup>6</sup>), 7.99 (d, *J* = 8.1 Hz, 1H, H<sup>1</sup>), 7.96 (d, *J* = 7.1 Hz, 1H, H<sup>12</sup>), 7.78 (dd, *J* = 8.0, 1.9 Hz, 1H, H<sup>20</sup>), 7.59 (d, *J* = 8.2 Hz, 1H, H<sup>9</sup>), 7.51 – 7.48 (m, 1H, H<sup>2</sup>), 7.47 – 7.44 (m, 1H, H<sup>4</sup>), 7.37 – 7.29 (m, 2H, H<sup>3</sup>, H<sup>10</sup>), 7.22 – 7.16 (m, 1H, H<sup>11</sup>), 4.23 (d, *J* = 95.0 Hz, 2H, 2H<sup>5</sup>), 3.62 – 3.55 (m, 4H, 2H<sup>25</sup>, 2H<sup>27</sup>), 3.53 (s, 2H, 2H<sup>22</sup>), 2.37 (d, *J* = 4.7 Hz, 4H, 2H<sup>24</sup>, 2H<sup>28</sup>). <sup>13</sup>C NMR (151 MHz, DMSO-*d*<sub>6</sub>) δ 155.51 (Cq, C<sup>7</sup>), 153.51 (Cq, C<sup>16</sup>), 152.01 (CH, C<sup>15</sup>), 149.72 ((CH, C<sup>18</sup>), 137.80 (Cq, C<sup>8a</sup>), 136.89 (CH, C<sup>20</sup>), 136.76 (Cq, C<sup>4a</sup>), 133.62 (Cq, C<sup>12c</sup>), 133.53 (Cq, C<sup>19</sup>), 129.03 (Cq, C<sup>7a</sup>), 128.09 (CH, C<sup>4</sup>), 128.05 (CH, C<sup>2</sup>), 127.41 (CH, C<sup>12</sup>), 126.32 (CH, C<sup>10</sup>), 124.94 (Cq, C<sup>12a</sup>), 124.09 (CH, C<sup>3</sup>), 120.45 (CH, C<sup>11</sup>), 120.34 (CH, C<sup>21</sup>), 120.20 (CH, C<sup>1</sup>), 117.07 (Cq, C<sup>12b</sup>), 112.68 (CH, C<sup>9</sup>), 66.16 (2CH<sub>2</sub>, C<sup>25</sup>, C<sup>27</sup>), 59.41 (CH<sub>2</sub>, C<sup>22</sup>), 53.09 (2CH<sub>2</sub>, C<sup>24</sup>, C<sup>28</sup>), 46.00 (CH<sub>2</sub>, C<sup>5</sup>). ESI-MS (acetonitrile/methanol + 1% water). positive: 451.21 [HL<sup>2</sup> + H]<sup>+</sup>, 901.28 [HL<sup>2</sup> + H]<sup>+</sup>.

**5,8-dihydroindolo[2,3-*d*][2]benzazepin-7(6*H*)-methylthione (10)**

Under argon flush sodium hydride (44mg, 1.83 mmol) was washed with hexane and dried *in vacuo*. 5,8-dihydroindolo[2,3-*d*][2]benzazepin-7(6*H*)-thione (**8**) (223.1 mg, 0.898 mmol) in THF<sub>dry</sub> (60 mL) was added and the solution was refluxed for 1 h. Methyl iodide (67.1 μL, 1.08 mmol) was added and the solution was refluxed for 2 h. The solution was cooled to room temperature and poured onto ice. The THF was removed under reduced pressure. The solution was extracted with dichloromethane (3 × 100 mL). The extract was concentrated and the raw product was purified on silica using a mixture of dichloromethane : methanol 99 : 1

as eluent. The product was obtained after evaporation of the solvent as a brown solid. Yield: 46.1 mg, 18%.  $^1\text{H NMR}$  (500 MHz, DMSO)  $\delta$  11.92 (s, 1H), 8.02 (d,  $J = 8.1$  Hz, 1H), 7.93 (d,  $J = 6.9$  Hz, 1H), 7.60 (d,  $J = 8.2$  Hz, 1H), 7.57 (d,  $J = 6.5$  Hz, 1H), 7.47 (td,  $J = 7.5, 1.4$  Hz, 1H), 7.38 (ddd,  $J = 13.0, 7.2, 1.1$  Hz, 2H), 7.24 (t,  $J = 7.1$  Hz, 1H), 5.03 (d,  $J = 10.7$  Hz, 1H), 3.78 (d,  $J = 9.5$  Hz, 1H), 2.43 (s, 3H). ESI-MS (acetonitrile/methanol + 1% water). positive: 279.10 [(**10**) + H] $^+$ .

### 3.3. Synthesis of metal complexes

The complexes to be newly designed are shown in Figure 20.

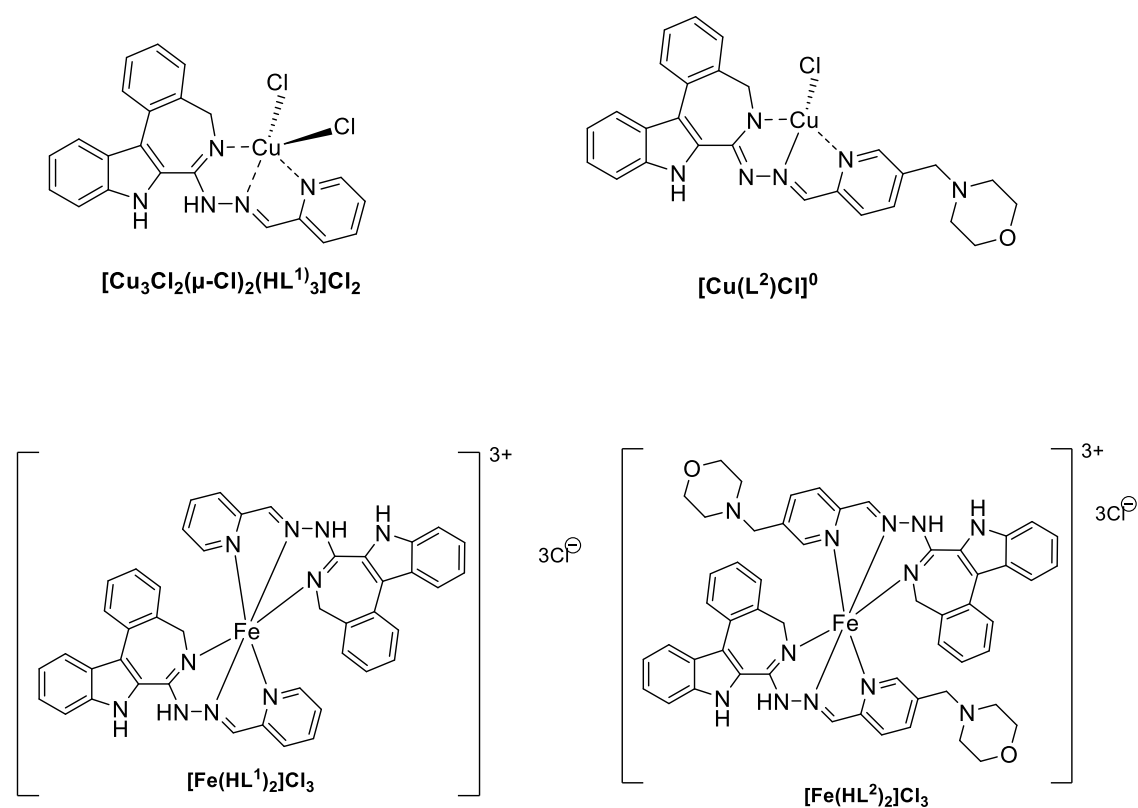


Figure 20: The four newly designed complexes; the structures for iron complexes are just suggestions since no x-ray could be conducted

#### (E)-7-(2-(pyridin-2-ylmethylene)hydrazineyl)-5,8-dihydroindolo[2,3-d][2]benzazepin-7-dichlorido-copper(II) $[\text{Cu}_3\text{Cl}_2(\mu\text{-Cl})_2(\text{HL}^1)_3]\text{Cl}_2$

(E)-7-(2-(pyridin-2-ylmethylene)hydrazineyl)-5,8-dihydroindolo[2,3-d][2]benzazepin(6H)one (**HL**<sup>1</sup>) (169 mg, 0.48 mmol) was dissolved in isopropanol (8 mL). A solution of copper(II) chloride (82 mg, 0.48 mmol) in methanol (0.5 mL) was added. The brown dispersion was heated to reflux for 1 h, cooled down and allowed to stand at 4 °C overnight. The product was filtered off and dried *in vacuo* to give a green-brown powder. Yield: 231.6mg, 99%. Anal. Calcd

for  $C_{22}H_{17}N_5CuCl_2 \cdot 0.4H_2O \cdot 0.7C_3H_8O$  ( $M = 535.13 \text{ g mol}^{-1}$ ): C, 53.86; H, 4.24, N, 13.08. Found: C, 54.09; H, 4.41; N, 13.08. Solubility in water between 1 and 1.5 mg mL<sup>-1</sup>. ESI-MS (acetonitrile/methanol + 1% water). positive: 352.16 [HL<sup>1</sup> + H]<sup>+</sup>, 764.18 [HL<sup>1</sup>CuL<sup>1</sup>]<sup>+</sup>. IR (ATR selected bands,  $\tilde{\nu}_{\text{max}}$ ): 2968, 2633, 3500 – 2500, 733 cm<sup>-1</sup>. UV-vis in 154 mM NaCl (34.4 μM),  $\lambda$ , nm, ( $\epsilon$ , M<sup>-1</sup> cm<sup>-1</sup>): 335 (12215), 470 (11101).

**(E)-4-((6-((2-(5,8-dihydroindolo[2,3-d][2]benzazepin-7-yl)hydrazineylidene)methyl)pyridin-3-yl)methyl)morpholine-dichlorido-copper(II) [Cu(L<sup>2</sup>)Cl]<sup>0</sup>**

To a solution of (E)-4-((6-((2-(5,8-dihydroindolo[2,3-d][2]benzazepin-7(6H)-yl)hydrazineylidene)methyl) pyridin-3-yl)methyl)morpholine (**HL<sup>2</sup>**) (203 mg, 0.45 mmol) in isopropanol (10 mL) a solution of copper(II) chloride dihydrate (77 mg, 0.45 mmol) dissolved in methanol (0.5 mL) was added. The mixture was heated to reflux for 1 h, cooled and allowed to stand in the fridge (4 °C) overnight. The product was filtered off and dried *in vacuo* to give a red brown-powder. Yield: 245 mg, 99%. Anal. Calcd for  $C_{27}H_{25}N_6OCuCl \cdot H_2O \cdot HCl$  ( $M = 603.00 \text{ g mol}^{-1}$ ): C, 53.9; H, 4.69, N, 13.98. Found: C, 53.98; H, 4.67; N, 13.79. Solubility in water: >4 mg mL<sup>-1</sup>. ESI-MS (acetonitrile/methanol + 1% water). positive: 512.14 [CuL<sup>2</sup>]<sup>+</sup>, 548.11 [CuHL<sup>2</sup>Cl]<sup>+</sup>, 553.14 [?]<sup>+</sup>, 962.32 [Cu(L<sup>2</sup>)<sub>2</sub> + H]<sup>+</sup>, 1061.21 [Cu<sub>2</sub>(L<sup>2</sup>)<sub>2</sub>Cl]<sup>+</sup>. IR (ATR selected bands,  $\tilde{\nu}_{\text{max}}$ ): 3500 – 2100, 1320, 1185, 775, 749 cm<sup>-1</sup>. UV-vis in 154 mM NaCl (25.2 μM),  $\lambda$ , nm, ( $\epsilon$ , M<sup>-1</sup> cm<sup>-1</sup>): 327 (12377), 465 (11675).

**bis[(E)-7-(2-(pyridin-2-ylmethylene)hydrazineyl)-5,8-dihydroindolo[2,3-d][2]benzazepin-7]-trichlorido-iron(III) [Fe(HL<sup>1</sup>)<sub>2</sub>]Cl<sub>3</sub>**

To a solution of (E)-7-(2-(pyridin-2-ylmethylene)hydrazineyl)-5,8-dihydroindolo[2,3-d][2]benzazepine (**HL<sup>1</sup>**) (117 mg, 0.33 mmol) in isopropanol (3 mL) iron(III) chloride hexahydrate (45 mg, 0.167 mmol) in methanol (0.5 mL) was added. The mixture was stirred for 2 h at room temperature and cooled overnight at 4°C. The product was filtered off and dried *in vacuo* to give a brown powder. Yield: 160 mg, 99% with crystal water included. Anal. Calcd for  $(C_{22}H_{17}N_5)_2FeCl_3 \cdot 1.3 H_2O$  ( $M = 888.43 \text{ g mol}^{-1}$ ): C, 59.48; H, 4.15, N, 15.77. Found: C, 59.46; H, 4.08; N, 15.48. Solubility in water: 1mg mL<sup>-1</sup> mg. ESI-MS (acetonitrile/methanol + 1% water). positive: 352,17 [H<sub>2</sub>L<sup>1</sup>]<sup>+</sup>, 756,20 [Fe(HL<sup>1</sup>)<sub>2</sub>]<sup>+</sup>. IR (ATR selected bands,  $\tilde{\nu}_{\text{max}}$ ): 1630, 1331,

1270, 1102, 736  $\text{cm}^{-1}$ . UV-vis in 154 mM NaCl (12.9  $\mu\text{M}$ ),  $\lambda$ , nm, ( $\epsilon$ ,  $\text{M}^{-1} \text{cm}^{-1}$ ): 342 (22248), 458 (13686).

**bis[(E)-4-((6-((2-(5,8-dihydroindolo[2,3-d][2]benzazepin-7-yl)hydrazineylidene)methyl)pyridin-3-yl)methyl)morpholine]-trichlorido-iron(III)  
[Fe(HL<sup>2</sup>)<sub>2</sub>]Cl<sub>3</sub>**

To a solution of (E)-4-((6-((2-(5,8-dihydroindolo[2,3-d][2]benzazepin-7(6H)-yl)hydrazineylidene)methyl)pyridin-3-yl)methyl)morpholine (**HL<sup>2</sup>**) (100 mg, 0.22 mmol) in isopropanol (2 mL) at 50 °C iron(III) chloride hexahydrate (30 mg, 0.11 mmol) in methanol (0.5 mL) was added. The mixture was stirred at 50 °C for 2 h and the product was precipitated with hexane. The mixture was allowed to stand in the fridge at 4 °C overnight. The product was filtered off and dried *in vacuo* to give a brown powder. Yield: 125.2 mg, 99% with crystal water included. Anal. Calcd for (C<sub>27</sub>H<sub>26</sub>N<sub>5</sub>)<sub>2</sub>FeCl<sub>3</sub>·5H<sub>2</sub>O·0.1C<sub>3</sub>H<sub>8</sub>O (M = 1159.36 g mol<sup>-1</sup>): C, 56.27; H, 5.5, N, 14.42. Found: C, 56.65; H, 5.27; N, 14.28. Solubility in water >5 mg mL<sup>-1</sup>. ESI-MS (acetonitrile/methanol + 1% water). positive: 954.33 [Fe(L<sup>2</sup>)<sub>2</sub>]<sup>+</sup>. IR (ATR selected bands,  $\tilde{\nu}_{\text{max}}$ ): 1607, 1327, 1106, 747  $\text{cm}^{-1}$ . UV-vis in 154 mM NaCl (12.8  $\mu\text{M}$ ),  $\lambda$ , nm, ( $\epsilon$ ,  $\text{M}^{-1} \text{cm}^{-1}$ ): 317 (32352), 423 (27406).

## 4. Results and Discussion

### 4.1. Synthesis of the organic scaffolds

Iodobenzonitrile and ethyl 1*H*-indole-2-carboxylate were used as starting materials to synthesise the indolobenzazepine backbone. The 1*H*-indole-2-carboxylate was first protected at the indole nitrogen with ethoxy-methylchloride (83% yield) and isolated as a light-yellow oil. Then the saponification was performed in 94% isolated yield. Upon fast cooling the product crystallises as voluminous, cloudy needles, whereas upon slow cooling the product crystallises as dense robust needles. The 2-Iodobenzonitrile was reduced to amine with 83% yield by using a tetrahydrofurane-borane complex as reductant. The amide coupling in dry dichloromethane was conducted straightforwardly with an almost quantitative yield. Under normal conditions, boc-protection gives almost quantitative yields in accord with the protocol by Putey et al. for exactly this reaction.<sup>105</sup> Various approaches have been conducted with

yields ranging from 67 to 83 %. It is unclear why the protection is not completely successful, although literature protocols were repeated. The next step, the intramolecular Heck reaction, produced high purity cyclised indolobenzazepine in quantitative yield. Worse yields have been received by using an MPLC-device with a short column. Quantitative yields were only received by doing the column by hand separating the products over 40 cm of silica. Although the product is white, hence, not visible on the column, it can be easily detected by testing the fluorescence on thin layer silica plates, because the fluorescence on the plates is more intense for the product than for the by-product. Deprotection of this moiety was proposed in two steps by Putey et al.: First, the Boc protection group can be cleaved under basic conditions with sodium hydroxide giving an intermediate in 80% yield; afterwards, the ethoxymethyl group can be removed under acidic conditions with 94% yield.<sup>105</sup> It is also known that the Boc-protection group is also susceptible to acidic cleavage. Therefore, these two steps were merged into one step only using hydrochloric acid to deprotect the scaffold completely, as also proposed for similar scaffolds by Putey et al.<sup>80</sup> The procedure only took half the time, since the basic deprotection is redundant. The product can be further purified by recrystallisation in methanol.

The thionation converting the lactam unit into a thiolactam unit was not straightforward. The first method used was the reaction with Lawesson's reagent in dry THF under argon atmosphere. This method failed even upon reflux overnight. However, by using basic aluminium oxide as a carrier for phosphorus(V) sulfide in acetonitrile<sup>116</sup> the thionation was performed with yield span from 50 to 83%. The yield increases with thoroughly grinded reactants. Insufficient adhesion of phosphorus(V) sulfide to the carrier might also lead to the inconsistent yields. The purification of this product has to be conducted carefully. The column needs to be long, since the product and the impurities, observed as a deep orange to red line, do not separate very well. For 1 gram crude product a column of 40 cm is recommended to get a good separation.

By the reaction of thiolactam **8** with excess hydrazine monohydrate used as reactant and solvent the hydrazine derivative **9** was prepared. The product precipitated from the solution as light yellow solid. One has only to take care that hydrazine itself is toxic and carcinogenic. The final Schiff bases **HL<sup>1</sup>** and **HL<sup>2</sup>** were both prepared in dry ethanol by condensation reaction of **9** with 2-picolylcarbaldehyde or 5-(morpholinomethyl)picolinaldehyde, respectively. Water

was used to precipitate the products. It was directly injected into the solution after the reaction was over, under normal conditions after one night at reflux. The generated precipitate was immediately dissolved by addition of ethanol. Concentration of the solution under reduced pressure lead to the precipitation of the product, which was easily separated by filtration and isolated in high yields and purity.

Ligand **L<sup>3</sup>** was not synthesised. Earlier research on related paullones showed no difficulty in its preparation.<sup>109,110</sup> The 5,8-dihydroindolo[2,3-*d*][2]benzazepine-7(6*H*)-thione did not show any conversion in dry THF with an excess of 2-picolylamine. No conversion was either observed in dry ethylacetate. Also using 2-picolylamine as solvent and reagent was tried. After the solvent was evaporated, it was taken up in ethylacetate and put in the fridge. The outcome has not yet been determined, since the product is too fine-grained to be filtered quantitatively. To make the thione more prone to the substrate, methylation of this functional group was accomplished. The procedure was published previously.<sup>109</sup> The product was only generated, when the sodium hydride suspension was freed from the surrounding oil and more than one and a half equivalents were taken, although the yield was very low (18%). Further reactions with this compound in 2-picolylamine are currently underway. Surprisingly, the thiolactam **9** reacted with the ruthenium(II)-arene dimer to give an unstable product,<sup>109</sup> which showed a peak in the ESI-MS with *m/z* 499.08 attributed to [**9**-H + Ru(II)arene]<sup>+</sup>. The purification and isolation of this compound was not successful during a variety of approaches, e.g. column chromatography or selective precipitation.

## 4.2. Copper(II) complexes

The synthesis of the desired copper complexes was performed by adapting the method of Primik et al.<sup>66</sup> Instead of addition of the methanolic solution of copper(II) chloride to a refluxing methanolic solution of the proligand, the proligand was dissolved in isopropanole and reacted with the copper(II) salt in methanol at room temperature. The reaction was completed by refluxing, even though the complex precipitated already at room temperature. The yield almost quantitative with excellent purity. The two copper(II) complexes differ in colour. Crystals of X-ray diffraction quality for the two compounds prepared were obtained by diethyl ether vapour diffusion into dimethylformamide solutions of the copper(II) complexes. The results of X-ray diffraction studies revealed that the copper(II) complex with **HL<sup>1</sup>** crystallised as a trimer  $[\text{Cu}_3\text{Cl}_2(\mu\text{-Cl})_2(\text{HL}^1)_3]\text{Cl}_2$  (Figure 21), while the second complex as

monomer of the general formula  $[\text{Cu}(\text{L}^2)\text{Cl}]^0$  (Figure 22). Selected bond distances are quoted in Tables 1 and 2, respectively.

Table 1: Bond lengths (Å) in the coordination polyhedron of copper(II) atoms in  $[\text{Cu}_3\text{Cl}_2(\mu\text{-Cl})_2(\text{HL}^1)_3]\text{Cl}_2$ .

	Bond lengths [Å]
<b>Cu1a-N6a</b>	1.997
<b>Cu1a-N14a</b>	1.991
<b>Cu1a-N17a</b>	2.046
<b>Cu1a-Cl<sub>a</sub></b>	2.268
<b>Cu1a-Cl<sub>ab</sub></b>	2.438
<b>Cu1b-N6b</b>	1.989
<b>Cu1b-N14b</b>	1.974
<b>Cu1b-N17b</b>	2.035
<b>Cu1b-Cl<sub>ab</sub></b>	2.449
<b>Cu1b-Cl<sub>bc</sub></b>	2.279
<b>Cu1c-N6c</b>	1.996
<b>Cu1c-N14c</b>	1.960
<b>Cu1c-N17c</b>	2.043
<b>Cu1c-Cl<sub>bc</sub></b>	2.639
<b>Cu1c-Cl<sub>d</sub></b>	2.212

Table 2: Bond lengths (Å) in the coordination polyhedron of copper(II) in  $[\text{Cu}(\text{L}^2)\text{Cl}]^0$

	Bond lengths [Å]
<b>Cu-N6</b>	1.947
<b>Cu-N14</b>	1.963
<b>Cu-N17</b>	2.020
<b>Cu-Cl</b>	2.236

The coordination geometry of three copper(II) atoms in the trimer can be described as distorted square-pyramidal. The extent of distortion is slightly different for the three copper(II) atoms and can be described by the  $\tau_5$ -parameter for five-coordinate complexes,<sup>117</sup> defined as  $(\text{Beta} - \text{Alpha})/60$ , which is equal to zero for a square-pyramidal coordination geometry and to one for a trigonal-bipyramidal coordination environment. The  $\tau_5$ -parameters for Cu1, Cu2 and Cu3 are as follows:  $157.83 - 142.87/60 = 0.25$ ,  $156.56 - 135.51/60 = 0.35$  and  $166.97 - 156.47/60 = 0.17$ , respectively. All three ligands are coordinated to copper(II) atoms in their neutral form via three nitrogen atoms. The coordination number 5 is completed by

two chloride-co-ligands. For Cub both coordinated chlorido co-ligands act as bridging ones to neighbouring copper(II) atoms Cua and Cuc. The global charge of the trimeric complex is counterbalanced by two chlorides as counteranions. In the second copper(II) complex with **HL<sup>2</sup>**, namely **[CuCl(L<sup>2</sup>)]<sup>0</sup>**, a square-planar coordination geometry is realised, in which the ligand is coordinated to copper(II) as monoanion via three nitrogen atoms and by one chloride as co-ligand. It should, however, be noted that one DMF molecule is approaching the apical position, but the Cu...O2 contact is long (2.589 Å) to be considered as an additional bond.

The IR-spectra of these two complexes show showed similar absorption peaks. The absorption in the area of 1500cm<sup>-1</sup> might reflect the stretching vibrations of the aromatic moieties or the deformation vibrations of the derivatised amide. The region around 3000 cm<sup>-1</sup> generally reflects aromatic, aliphatic and amine vibrations fitting well into the scaffold. The characteristic water peak at 1600cm<sup>-1</sup> and above is missing, indicating dry product. Characteristic peaks appear for **[Cu<sub>3</sub>Cl<sub>2</sub>(μ-Cl)<sub>2</sub>(HL<sup>1</sup>)<sub>3</sub>]Cl<sub>2</sub>** at 2968 cm<sup>-1</sup> and 2633 cm<sup>-1</sup> within a broad band from around 3500 cm<sup>-1</sup> to 2500 cm<sup>-1</sup>, and 733 cm<sup>-1</sup>. For **[Cu(L<sup>2</sup>)Cl]<sup>0</sup>** the broad band is not that intensive, some characteristics are striking bands at 1320 cm<sup>-1</sup> and 1112 cm<sup>-1</sup>. The solubility of these two complexes in water including 1% DMSO differs tremendously. **[Cu<sub>3</sub>Cl<sub>2</sub>(μ-Cl)<sub>2</sub>(HL<sup>1</sup>)<sub>3</sub>]Cl<sub>2</sub>** can be dissolved in this mixture between 1 and 1.5 mg/mL. The solubility of **[Cu(L<sup>2</sup>)Cl]<sup>0</sup>** is determined to be higher than 4 mg/mL. This improvement in solubility may derive from the influences of the ligand. The ligand itself bears a morpholine unit, which is supposed to increase the pharmacological profile, including the solubility.<sup>112,113</sup> Moreover, this ligand forced the complexation geometry to be square planar. This might also contribute to the improved properties. For **[Cu<sub>3</sub>Cl<sub>2</sub>(μ-Cl)<sub>2</sub>(HL<sup>1</sup>)<sub>3</sub>]Cl<sub>2</sub>** the thermogravimetric analysis (TGA) showed two distinct changes in the structure. From 150 to 200°C a loss of mass of around 9% is visible. This is probably a loss of HCl. The second change starts at 200°C and lasts until 500°C. This loss of mass cannot be further described. For **[Cu(L<sup>2</sup>)Cl]<sup>0</sup>**, the loss of HCl is not visible. Two exothermic reactions can be observed, one at 220°C and the other one at 370°C. Afterwards a possible decomposition is visible since the mass is reduced drastically.

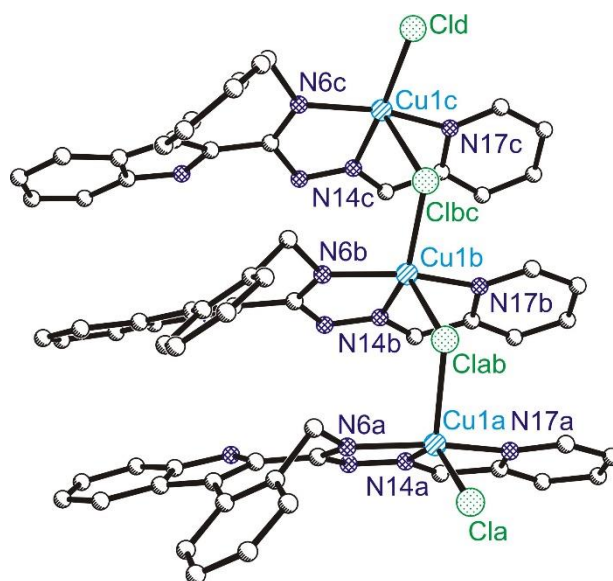


Figure 21: X-ray diffraction structure of  $[\text{Cu}_3\text{Cl}_2(\mu\text{-Cl})_2(\text{HL}^1)_3]\text{Cl}_2$ ; blue represents copper, violet represents nitrogen, green represents chlorine.

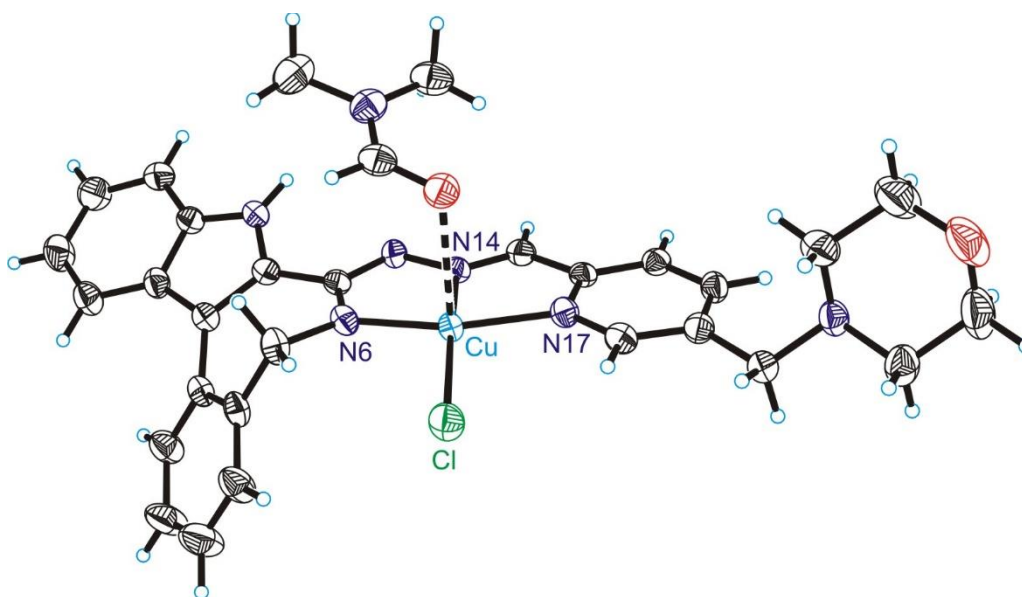


Figure 22: X-ray diffraction structure of  $[\text{Cu}(\text{L}^2)\text{Cl}]^0$ ; blue represents copper, violet represents nitrogen, red represents oxygen, green represents chlorine.

### 4.3. Iron(III) complexes

The iron(III) complexes  $[\text{Fe}(\text{HL}^1)_2]\text{Cl}_3$  and  $[\text{Fe}(\text{HL}^2)_2]\text{Cl}_3$  were prepared by reaction of  $\text{FeCl}_3 \cdot 6\text{H}_2\text{O}$  with the corresponding proligand in 1 : 2 mole ratio in isopropanol.  $[\text{Fe}(\text{HL}^2)_2]\text{Cl}_3$  was precipitated from the reaction mixture with hexane. Both complexes were isolated in excellent yields and purity, although the weight of the product exceeded the theoretical yield. Elemental analysis indicates the presence of co-crystallised water molecules. Attempts to grow single crystals suitable for X-ray diffraction failed. The TGAs of both iron complexes

highly suggest the presence of crystal water molecules.  $[\text{Fe}(\text{HL}^1)_2]\text{Cl}_3$  shows a loss of around 12% mass up to 200°C, which represents the mass equivalent of the six molecules of water, although elemental analysis suggests only 1.3 molecules of water. One reason for this might be that the product was humid while being measured. At 325°C one exothermic reaction takes place, which can be assigned to the formation of iron oxide and the loss of ligand  $[\text{Fe}(\text{HL}^2)_2]\text{Cl}_3$  shows similar behaviour. Six molecules of water can be assigned to the first loss of weight, although this loss takes place in two steps summarizing to 10.5% up to 240°C. Afterwards the product decomposes as well. Surprisingly, three exothermic reactions can be observed: one at 180°C, the second one at around 320°C and the last one at 360°C. Again, it is visible that the additional morpholine group has great impacts on the behaviour of the complexes.

The structural properties of these two complexes can only be assumed by now. It is suggested that the ligands are not deprotonated and three chloride counterions are present. IR-spectra of both complexes look similar. Nevertheless, some striking differences can be observed.  $[\text{Fe}(\text{HL}^1)_2]\text{Cl}_3$  shows a broad absorption band from 3500 to 2500  $\text{cm}^{-1}$ .  $[\text{Fe}(\text{HL}^2)_2]\text{Cl}_3$  shows the same band as well but it is more intense and broadens down to around 2100  $\text{cm}^{-1}$ . These absorptions can be linked with amine and amide, as well as aromatic vibrations. The area from 1630  $\text{cm}^{-1}$  down to the fingerprint area are dominated by sharp peaks. For  $[\text{Fe}(\text{HL}^1)_2]\text{Cl}_3$  bands at 1630  $\text{cm}^{-1}$ , 1331  $\text{cm}^{-1}$ , 1270  $\text{cm}^{-1}$ , 1102  $\text{cm}^{-1}$  and 736  $\text{cm}^{-1}$  are characteristic.  $[\text{Fe}(\text{HL}^2)_2]\text{Cl}_3$  shows characteristic bands at 1607  $\text{cm}^{-1}$ , 1327  $\text{cm}^{-1}$ , 1106  $\text{cm}^{-1}$  and 747  $\text{cm}^{-1}$ . The increased intensity of  $[\text{Fe}(\text{HL}^2)_2]\text{Cl}_3$  in the area around 3000  $\text{cm}^{-1}$  could be attributed to morpholine group. Concerning the solubility, the same trends are observable as seen with the copper(II) complexes.  $[\text{Fe}(\text{HL}^1)_2]\text{Cl}_3$  is soluble only up to 1 mg/mL in water with 1% DMSO, whereas  $[\text{Fe}(\text{HL}^2)_2]\text{Cl}_3$  is soluble more than 5 mg/mL. Without knowing the crystal structures this effect can only be attributed to the additional morpholine group in  $[\text{Fe}(\text{HL}^2)_2]\text{Cl}_3$ .

#### 4.4. UV-vis measurements

The UV-vis measurements of the four complexes in 154 mM NaCl solution do not differ very much. It is of note that all complexes show decreased absorbance over time, which is due to the precipitation of the complexes. Nevertheless, the precipitation can be easily redissolved.

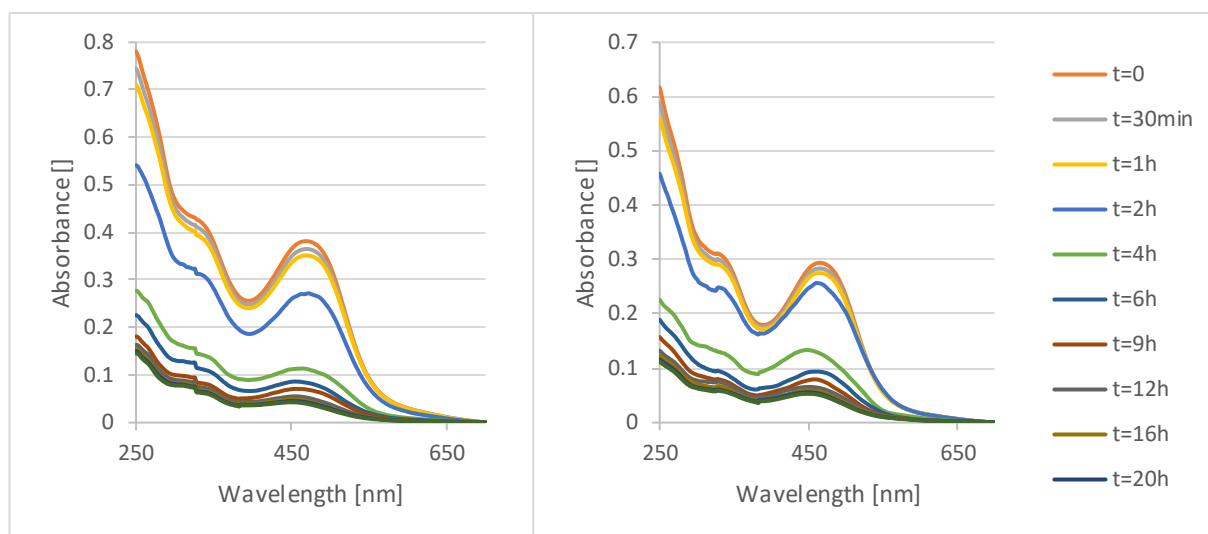


Figure 23: UV-vis measurements over time from 0 to 20 hours; left:  $[\text{Cu}_3\text{Cl}_2(\mu\text{-Cl})_2(\text{HL}^1)_3]\text{Cl}_2$ , right:  $[\text{Cu}(\text{L}^2)\text{Cl}]^0$  in 154 mM NaCl

A comparison can be drawn between the ligand  $\text{L}^1$  and  $\text{L}^2$ , and the four complexes synthesised. The ligands themselves are not soluble in water and 1% DMSO. Upon complexation, this changed dramatically, since the complexes  $[\text{Cu}_3\text{Cl}_2(\mu\text{-Cl})_2(\text{HL}^1)_3]\text{Cl}_2$  and  $[\text{Fe}(\text{HL}^1)_2]\text{Cl}_3$  have similar solubilities of 1 mg/mL. This effect is even enhanced for the complexes  $[\text{Cu}(\text{L}^2)\text{Cl}]^0$  and  $[\text{Fe}(\text{HL}^2)_2]\text{Cl}_3$ , which are soluble up to more than 4 mg/mL. This confirms the solubility enhancement due to the attachment of the morpholine moiety as well as complex formation.

#### 4.5. Electrochemical behaviour

Detailed electrochemical studies were performed using cyclic voltammetry, as well as UV-vis-spectroelectrochemistry to investigate the redox properties of the complexes synthesised,  $[\text{Cu}_3\text{Cl}_2(\mu\text{-Cl})_2(\text{HL}^1)_3]\text{Cl}_2$ ,  $[\text{Cu}(\text{L}^2)\text{Cl}]^0$ ,  $[\text{Fe}(\text{HL}^1)_2]\text{Cl}_3$  and  $[\text{Fe}(\text{HL}^2)_2]\text{Cl}_3$ . For the cyclic voltammograms DMSO/ $n\text{Bu}_4\text{NPF}_6$  was used in combination with a glassy carbon (GC) working electrode at a scan rate of  $100 \text{ mV s}^{-1}$ . The reference for the redox potentials was the ferrocenium/ferrocene couple ( $\text{Fc}^+/\text{Fc}$ ). For the spectroelectrochemical UV-vis measurements a microstructured honeycomb platinum electrode was used at a scan rate of  $10 \text{ mV s}^{-1}$ . Both analyses were conducted under argon atmosphere.

The cyclic voltammogram of  $[\text{Cu}_3\text{Cl}_2(\mu\text{-Cl})_2(\text{HL}^1)_3]\text{Cl}_2$  shows two irreversible reduction peaks at cathodic potentials of  $E_{\text{pc}} = -0.75 \text{ V}$  and at  $E_{\text{pc}} = -1.13 \text{ V}$  vs.  $\text{Fc}^+/\text{Fc}$ . (Figure 24a). The first reduction step can be assigned to the  $\text{Cu}(\text{II}) \rightarrow \text{Cu}(\text{I})$  reduction. It is supposed that the complex containing copper(I) is not stable, therefore, it decomposes with partial or complete ligand

release. This product is presumably further irreversibly reduced to Cu(0). For the second copper complex,  $[\text{Cu}(\text{L}^2)\text{Cl}]^0$ , irreversible redox character was observed as well with only one cathodic peak at  $E_{\text{pc}}^1 = -1.07 \text{ V vs. Fc}^+/\text{Fc}$  (Figure 24b). Similar to  $[\text{Cu}_3\text{Cl}_2(\mu\text{-Cl})_2(\text{HL}^1)_3]\text{Cl}_2$ ,  $[\text{Cu}(\text{L}^2)\text{Cl}]^0$  decomposes upon reduction.

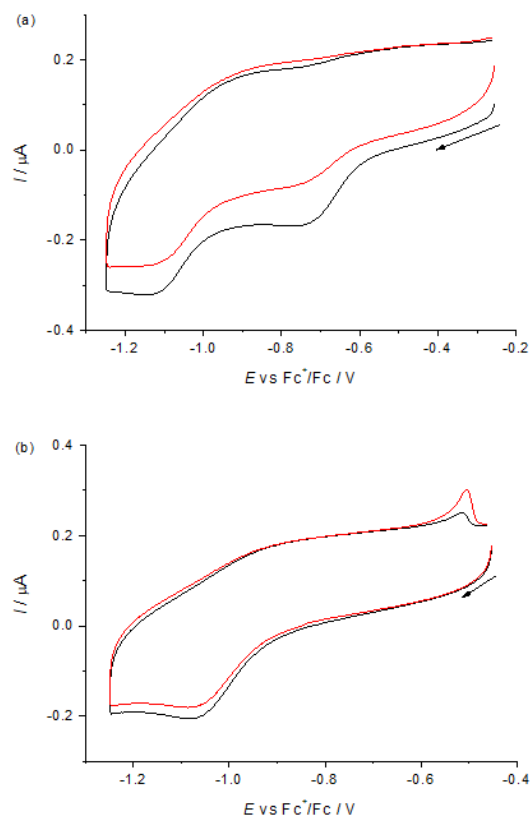


Figure 24: Cyclic voltammograms of (a)  $[\text{Cu}_3\text{Cl}_2(\mu\text{-Cl})_2(\text{HL}^1)_3]\text{Cl}_2$  and (b)  $[\text{Cu}(\text{L}^2)\text{Cl}]^0$  in DMSO/ $n\text{Bu}_4\text{NPF}_6$  at scan rate of  $100 \text{ mV s}^{-1}$  and at GC working electrode (black traces represent the first scan, while red traces the second scan).

To investigate if the first reduction step of the copper(II) complexes is chemically reversible, UV-vis measurements were conducted. It revealed that upon reduction of  $[\text{Cu}_3\text{Cl}_2(\mu\text{-Cl})_2(\text{HL}^1)_3]\text{Cl}_2$  a new optical band arises at 385 nm in addition to the decrease in intensity for the optical bands at 275 and 485 nm, respectively (see Figure 25).

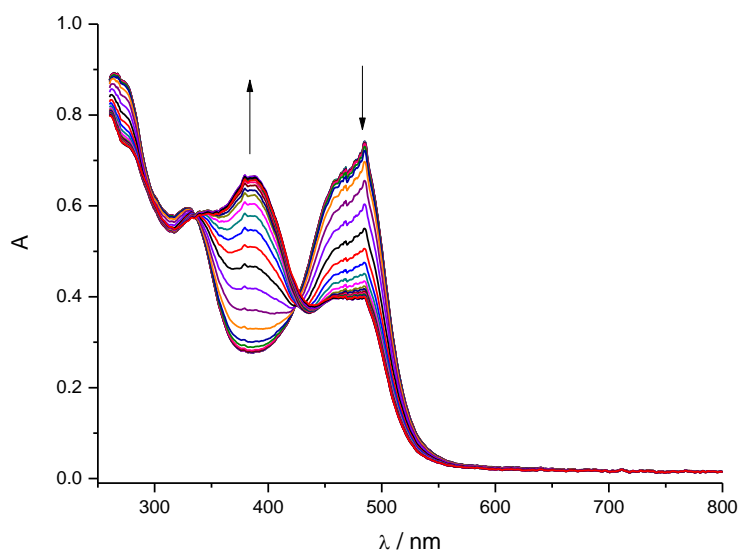


Figure 25: Evolution of UV-vis spectra in 2D projection in forward scan observed for  $[\text{Cu}_3\text{Cl}_2(\mu\text{-Cl})_2(\text{HL}^1)_3]\text{Cl}_2$  in  $\text{DMSO}/n\text{Bu}_4\text{NPF}_6$  in the region of the first cathodic peak (scan rate of  $10 \text{ mV s}^{-1}$ , Pt-microstructured honeycomb working electrode).

Similar results were observed for  $[\text{Cu}(\text{L}^2)\text{Cl}]^0$ , since a new optical band at 389 nm is generated upon reduction (Figure 26a). Upon scan reversal, however, the product formed upon the the reduction of Cu(II) to Cu(I) does not exhibit reoxidation to copper(II) (Figure 26b). Thus, evidence is provided that the Cu(I) complex is not stable and further decomposes with ligand release. Previous research conducted by Milunović et al. suggested that this kind of ligand is able to act as iron chelator with inhibition of the R2-RNR enzyme essential for the DNA synthesis and highly expressed in cancer cells.<sup>118</sup> Since the complex decomposes, copper(I) is released in the cells contributing to the production of ROS and consequently to Fenton-like kinetics.

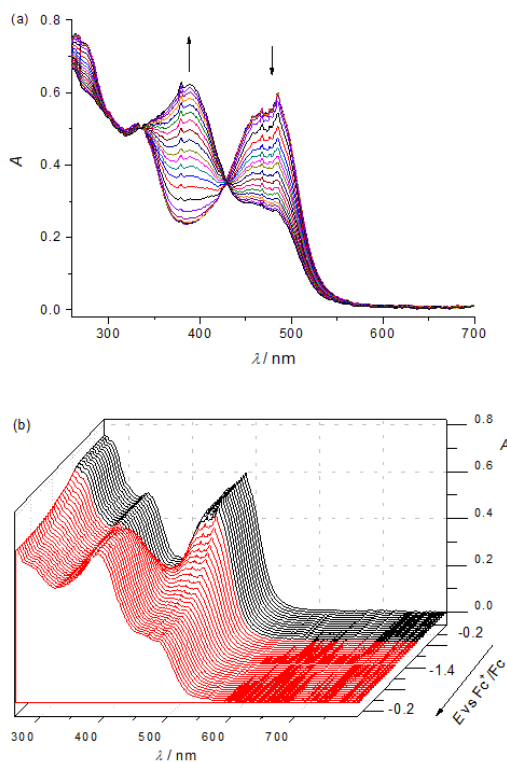


Figure 26: In situ UV-vis-NIR spectroelectrochemistry for  $[\text{Cu}(\text{L}^2)\text{Cl}]^0$  in  $\text{DMSO}/n\text{Bu}_4\text{NPF}_6$  (scan rate of  $10 \text{ mV s}^{-1}$ , Pt-microstructured honeycomb working electrode): (a) evolution of UV-vis spectra in 2D projection in forward scan; (b) UV-vis spectra detected simultaneously upon the cyclic voltammetric scan in 3D projection.

In contrast to the copper(II) complexes  $[\text{Cu}_3\text{Cl}_2(\mu\text{-Cl})_2(\text{HL}^1)_3]\text{Cl}_2$  and  $[\text{Cu}(\text{L}^2)\text{Cl}]^0$ , the iron(III) complexes  $[\text{Fe}(\text{HL}^1)_2]\text{Cl}_3$  and  $[\text{Fe}(\text{HL}^2)_2]\text{Cl}_3$  exhibit very different redox behaviours with almost reversible reduction. Interestingly, the first reduction for  $[\text{Fe}(\text{HL}^2)_2]\text{Cl}_3$  takes place at a half wave potential of  $E_{1/2} = -0.37 \text{ V vs. Fc}^+/\text{Fc}$  (see Figure 27a) and for  $[\text{Fe}(\text{HL}^1)_2]\text{Cl}_3$  at a half wave potential of  $E_{1/2} = -0.48 \text{ V vs. Fc}^+/\text{Fc}$  (see Figure 27b). It is notable that the peak at  $-0.32 \text{ V vs. Fc}^+/\text{Fc}$  for  $[\text{Fe}(\text{HL}^1)_2]\text{Cl}_3$  is for now attributed to an oxidation process of the initial complex, which will be discussed below.

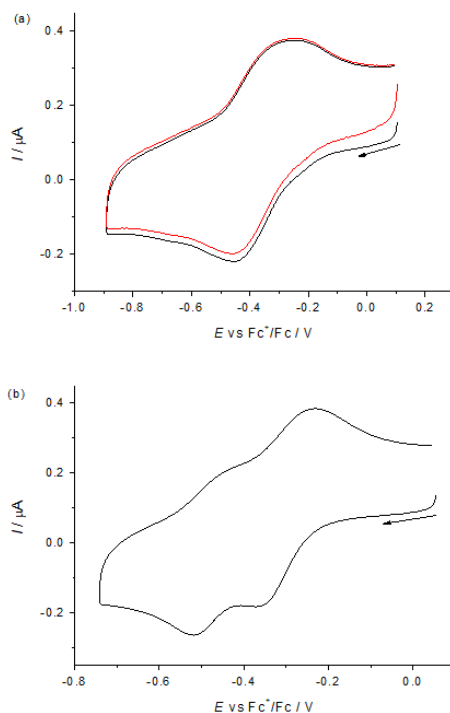


Figure 27: Cyclic voltammograms of iron complexes (a)  $[\text{Fe}(\text{HL}^2)_2]\text{Cl}_3$  and (b)  $[\text{Fe}(\text{HL}^1)_2]\text{Cl}_3$  in  $\text{DMSO}/n\text{Bu}_4\text{NPF}_6$  at scan rate of  $100 \text{ mV s}^{-1}$  and at GC working electrode (black traces represent the first scan, while red trace the second scan).

Upon the first cathodic reduction of complex  $[\text{Fe}(\text{HL}^2)_2]\text{Cl}_3$  new optic absorption bands arise at 406 and 658 nm, creating an isosbestic point at 580 nm (see Figure 28a). The low intensity band at 658 nm is characteristic for iron(II) complexes (see supporting information of Ohui, K. et al.<sup>119</sup>). This confirms the reduction of iron(III) to iron(II). In addition, almost full recovery of the initial optical bands was observed upon voltammetric reverse scan. This is evidence for the chemical reversibility of the redox reaction even at low scan rates (see Figure 28b).

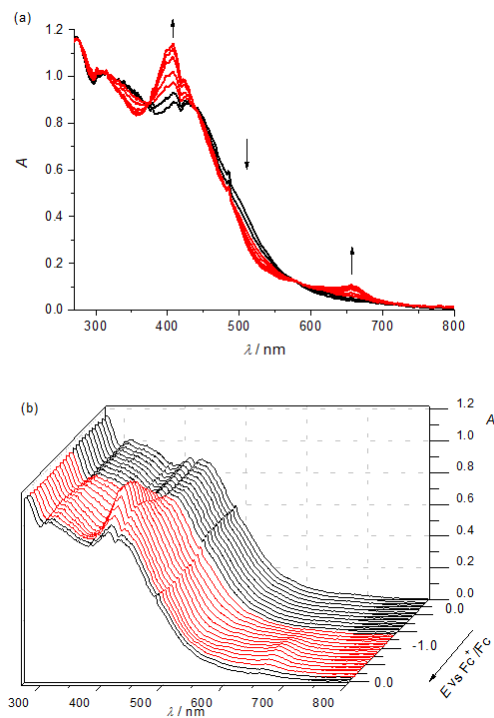


Figure 28: Spectroelectrochemistry of  $[\text{Fe}(\text{HL}^2)_2]\text{Cl}_3$  in  $n\text{Bu}_4\text{NPF}_6/\text{DMSO}$  in the region of the first cathodic peak. (a) UV-vis spectra detected simultaneously during the in-situ reduction (Pt-microstructured honeycomb working electrode, scan rate  $v = 10 \text{ mV s}^{-1}$ ); (b) potential dependence of UV-vis spectra.

These redox active complexes have the ability to increase the amount of ROS generated by undergoing Fenton-kinetics based on the reversible redox behaviour of Fe(II)/Fe(III).<sup>119</sup>

For  $[\text{Fe}(\text{HL}^1)_2]\text{Cl}_3$  similar changes were observed in the region of the second reduction peak at around  $-0.5 \text{ V vs. Fc}^+/\text{Fc}$ , visible in Figure 29a. Upon the reduction of the complex a new optical band arises at 656 nm indicating the generation of an iron(II) species. It is worth noting that the oxidation process taking place at a potential around  $0.0 \text{ V vs. Fc}^+/\text{Fc}$  in  $[\text{Fe}(\text{HL}^1)_2]\text{Cl}_3$  was observed with high positive currents. However, no changes were observable in the UV-vis range from 300 to 1000 nm (see Figure 29b), indicating that the oxidation process at around  $0.0 \text{ V vs. Fc}^+/\text{Fc}$  is ligand based, since the second cathodic peak corresponds well with the other anodic peak.

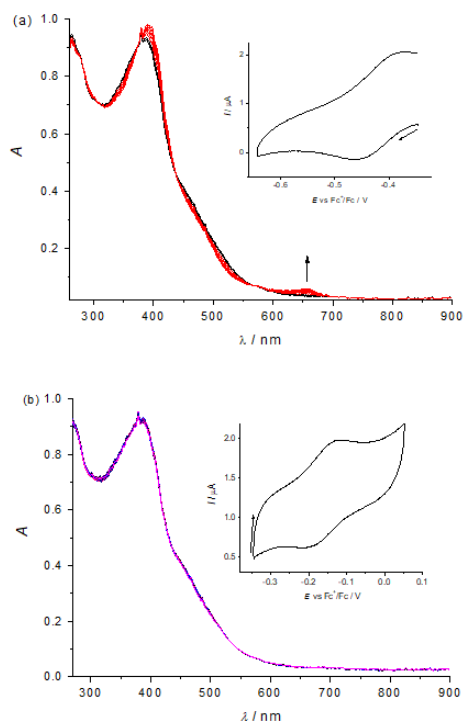


Figure 29: UV-vis spectra detected simultaneously during spectroelectrochemistry of  $[\text{Fe}(\text{HL}^1)_2]\text{Cl}_3$  in  $n\text{Bu}_4\text{NPF}_6/\text{DMSO}$  (a) in the region of the first cathodic peak and (b) in the region of the first anodic peak (insets: corresponding cyclic voltammograms, Pt-microstructured honeycomb working electrode, scan rate  $v = 5 \text{ mV s}^{-1}$ ).

## 5. Conclusion

A new class of potential metal-based anticancer drugs has been synthesised and characterised. The synthesis of the main organic scaffold was performed in seven steps. The creation of binding sites able to accommodate metal ions was realised in three additional steps. The thionation step was improved by using phosphorus(V) sulfide instead of Lawesson's reagent to make the scaffold reactive enough for the following reaction with hydrazine. The Schiff base reactions afforded straightforwardly excellent quality and yields of proligands  $\text{HL}^1$  and  $\text{HL}^2$ . The synthesis of proligand  $\text{L}^3$  did not work, although several different pathways were explored to facilitate the final reaction with 2-picolylamine, e.g. methylation of the thiolactam (**8**). Only low conversion could be achieved, even though the compound was not isolated and characterised.

Two copper(II) complexes were synthesised.  $[\text{Cu}_3\text{Cl}_2(\mu\text{-Cl})_2(\text{HL}^1)_3]\text{Cl}_2$  was isolated as a green-brown powder which crystallised as a trimer bridged by chlorido co-ligands with two chlorides as counterions. The coordination geometry for all three copper(II) ions is slightly distorted square-pyramidal. The second compound,  $[\text{Cu}(\text{L}^2)\text{Cl}]^0$ , was isolated as a red-brown powder. Its

coordination geometry is square-planar, even though weak coordination of DMF in apical position can be admitted ( $\text{Cu} - \text{O} = 2.589 \text{ \AA}$ ).  $\text{HL}^2$  acts as monoanion in the complex, in contrast to  $\text{HL}^1$ , which remains in the same protonated state in the trimer. The electrochemistry of the two copper(II) complexes is similar. Their electrochemical reduction is irreversible. It is suggested that upon reduction of the central ion the ligands can be released. No Fenton-like kinetics could be observed due to the irreversible behaviour of these copper(II) compounds.

In addition, two iron(III) complexes  $[\text{Fe}(\text{HL}^1)_2]\text{Cl}_3$  and  $[\text{Fe}(\text{HL}^2)_2]\text{Cl}_3$  were successfully prepared. The molar ratio between iron(III) and the respective ligands is 1 : 2, which is confirmed by the ESI mass spectra. Octahedral coordination geometry for these two complexes was proposed. The electrochemical behaviour of iron(III) complexes is different from that of copper(II) compounds.  $[\text{Fe}(\text{HL}^1)_2]\text{Cl}_3$  and  $[\text{Fe}(\text{HL}^2)_2]\text{Cl}_3$  show reversible redox behaviour. The iron(II) congener is obtained upon reduction in the biologically accessible potential range, which is confirmed by spectroelectrochemical analysis. This redox reversibility is supposed to generate ROS by mainly preserving the structure of the complex.

## 6. References

- 1 From Statistik Austria: An Bösartigen Neubildungen ( ICD-Codes : C00-C97 ) Gestorbene seit 1970 nach Geschlecht und Bundesländern ( absolut und altersstandardisierte Sterberaten ), [https://www.statistik.at/web\\_de/statistiken/menschen\\_und\\_gesellschaft/gesundheit/todesursachen/todesursachen\\_ausgewaehlte/index.html](https://www.statistik.at/web_de/statistiken/menschen_und_gesellschaft/gesundheit/todesursachen/todesursachen_ausgewaehlte/index.html), (accessed 4 January 2019).
- 2 From Statistik Austria: Malignome, insgesamt (C00-C97, ohne C44) - Krebsinzidenz (Neuerkrankungen pro Jahr), Österreich ab 1983, [https://www.statistik.at/web\\_de/statistiken/menschen\\_und\\_gesellschaft/gesundheit/krebserkrankungen/krebs\\_im\\_ueberblick/index.html](https://www.statistik.at/web_de/statistiken/menschen_und_gesellschaft/gesundheit/krebserkrankungen/krebs_im_ueberblick/index.html), (accessed 4 January 2019).
- 3 From the World Health Organisation: All cancers, <http://gco.iarc.fr/today/fact-sheets-cancers>, (accessed 7 January 2019).
- 4 From Statistik Austria: Krebsinzidenz (Neuerkrankungen) im Kindes und Jugendalter, Österreich 2002-2012, [https://www.statistik.at/web\\_de/statistiken/menschen\\_und\\_gesellschaft/gesundheit/krebserkrankungen/krebs\\_bei\\_kindern-und\\_jugendlichen/index.html](https://www.statistik.at/web_de/statistiken/menschen_und_gesellschaft/gesundheit/krebserkrankungen/krebs_bei_kindern-und_jugendlichen/index.html), (accessed 4 January 2019).
- 5 From Statistik Austria: Bevölkerung zu Jahresbeginn seit 1981 nach Geschlecht, breiten Altersklassen und Staatsangehörigkeit,

- [https://www.statistik.at/web\\_de/statistiken/menschen\\_und\\_gesellschaft/bevoelkerung/bevoelkerungsstand\\_und\\_veraenderung/bevoelkerungsveraeenderung\\_nach\\_komponenten/index.html](https://www.statistik.at/web_de/statistiken/menschen_und_gesellschaft/bevoelkerung/bevoelkerungsstand_und_veraenderung/bevoelkerungsveraeenderung_nach_komponenten/index.html), (accessed 30 January 2019).
- 6 From Statistik Austria: Malignome, insgesamt (C00-C97, ohne C44) - Krebsinzidenz nach Stadium, Jahresdurchschnitt (2013/2015),  
[https://www.statistik.at/web\\_de/statistiken/menschen\\_und\\_gesellschaft/gesundheit/krebserkrankungen/krebs\\_im\\_ueberblick/index.html](https://www.statistik.at/web_de/statistiken/menschen_und_gesellschaft/gesundheit/krebserkrankungen/krebs_im_ueberblick/index.html), (accessed 4 January 2019).
  - 7 From Statistik Austria: M. Hackl, A. Hanika, J. Klotz, B. Leitner and N. Zielonke, Trends der Entwicklung von Krebserkrankungen in Österreich, eine Prognose bis 2030,  
[https://www.statistik.at/web\\_de/statistiken/menschen\\_und\\_gesellschaft/gesundheit/krebserkrankungen/prognose\\_krebsinzidenz\\_krebsmortalitaet/index.html](https://www.statistik.at/web_de/statistiken/menschen_und_gesellschaft/gesundheit/krebserkrankungen/prognose_krebsinzidenz_krebsmortalitaet/index.html), (accessed 4 January 2019).
  - 8 From Statistik Austria: Entwicklung der Krebsprävalenz im Zeitverlauf, Österreich ab 2001,  
[https://www.statistik.at/web\\_de/statistiken/menschen\\_und\\_gesellschaft/gesundheit/krebserkrankungen/krebspraevalenz/index.html](https://www.statistik.at/web_de/statistiken/menschen_und_gesellschaft/gesundheit/krebserkrankungen/krebspraevalenz/index.html), (accessed 4 January 2019).
  - 9 From Statistik Austria: Krebsprävalenz am 31.12.2015, nach ausgewählten Krebslokalisationen und Geschlecht,  
[https://www.statistik.at/web\\_de/statistiken/menschen\\_und\\_gesellschaft/gesundheit/krebserkrankungen/krebspraevalenz/index.html](https://www.statistik.at/web_de/statistiken/menschen_und_gesellschaft/gesundheit/krebserkrankungen/krebspraevalenz/index.html), (accessed 4 January 2019).
  - 10 From Statistik Austria: M. Hackl, A. Hanika and J. Klotz, Prognose der Krebsprävalenz bis 2030,  
[https://www.statistik.at/web\\_de/statistiken/menschen\\_und\\_gesellschaft/gesundheit/krebserkrankungen/prognose\\_der\\_krebspraevalenz/index.html](https://www.statistik.at/web_de/statistiken/menschen_und_gesellschaft/gesundheit/krebserkrankungen/prognose_der_krebspraevalenz/index.html), (accessed 27 December 2018).
  - 11 From Statistik Austria: Krebsmortalität (Sterbefälle) im Kindes und Jugendalter, Österreich 2002-2012,  
[https://www.statistik.at/web\\_de/statistiken/menschen\\_und\\_gesellschaft/gesundheit/krebserkrankungen/krebs\\_bei\\_kindern-und\\_jugendlichen/index.html](https://www.statistik.at/web_de/statistiken/menschen_und_gesellschaft/gesundheit/krebserkrankungen/krebs_bei_kindern-und_jugendlichen/index.html), (accessed 4 January 2019).
  - 12 From Statistik Austria: Ergebnisse im Überblick: Relatives Überleben,  
[https://www.statistik.at/web\\_de/statistiken/menschen\\_und\\_gesellschaft/gesundheit/krebserkrankungen/ueberleben\\_mit\\_krebs/index.html](https://www.statistik.at/web_de/statistiken/menschen_und_gesellschaft/gesundheit/krebserkrankungen/ueberleben_mit_krebs/index.html), (accessed 4 January 2019).
  - 13 From Statistik Austria: 5-Jahres relatives Überleben in Österreich zwischen 1988 und 2012 nach Alter und Geschlecht,  
[https://www.statistik.at/web\\_de/statistiken/menschen\\_und\\_gesellschaft/gesundheit/krebserkrankungen/ueberleben\\_mit\\_krebs/index.html](https://www.statistik.at/web_de/statistiken/menschen_und_gesellschaft/gesundheit/krebserkrankungen/ueberleben_mit_krebs/index.html)

- krankungen/ueberleben\_mit\_krebs/index.html, (accessed 4 January 2019).
- 14 From Statistik Austria: Malignome, insgesamt (C00-C97, ohne C44) - Relative Überlebensraten in Österreich nach Geschlecht (1988- 2015), [https://www.statistik.at/web\\_de/statistiken/menschen\\_und\\_gesellschaft/gesundheit/krebserkrankungen/krebs\\_im\\_ueberblick/index.html](https://www.statistik.at/web_de/statistiken/menschen_und_gesellschaft/gesundheit/krebserkrankungen/krebs_im_ueberblick/index.html), (accessed 4 January 2019).
  - 15 From Statistik Austria: Beobachtete 5-Jahres-Überlebensraten im Kindes und Jugendalter nach Krebslokalisationen , Österreich Beobachtete 5-Jahres-Überlebensraten im Kindes und Jugendalter nach Krebslokalisationen , Österreich, [https://www.statistik.at/web\\_de/statistiken/menschen\\_und\\_gesellschaft/gesundheit/krebserkrankungen/krebs\\_bei\\_kindern-und\\_jugendlichen/index.html](https://www.statistik.at/web_de/statistiken/menschen_und_gesellschaft/gesundheit/krebserkrankungen/krebs_bei_kindern-und_jugendlichen/index.html), (accessed 4 January 2019).
  - 16 From Statistik Austria: Gestorbene nach Todesursachen seit 1945, [https://www.statistik.at/web\\_de/statistiken/menschen\\_und\\_gesellschaft/gesundheit/todesursachen/todesursachen\\_im\\_ueberblick/index.html](https://www.statistik.at/web_de/statistiken/menschen_und_gesellschaft/gesundheit/todesursachen/todesursachen_im_ueberblick/index.html), (accessed 4 January 2019).
  - 17 O. Warburg, *Science (80- )*, 1956, **123**, 309–314.
  - 18 Nowell P. C., *Science (80- )*, 1976, **194**, 23–28.
  - 19 A Brief Guide to Genomics, <https://www.genome.gov/18016863/a-brief-guide-to-genomics/>, (accessed 9 January 2019).
  - 20 D. Hanahan and R. Weinberg, *Cell*, 2000, **100**, 57–70.
  - 21 D. Hanahan and R. Weinberg, *Cell*, 2011, **144**, 646–674.
  - 22 Y. A. Fouad and C. Aanei, *Am. J. Cancer Res.*, 2017, **7**, 1016–1036.
  - 23 G. Housman, S. Byler, S. Heerboth, K. Lapinska, M. Longacre, N. Snyder and S. Sarkar, *Cancers (Basel)*, 2014, **6**, 1769–1792.
  - 24 K. J. Harrington, *Medicine (Baltimore)*, 2011, **39**, 689–692.
  - 25 L. E. Heasley, *Oncogene*, 2001, **20**, 1563–1569.
  - 26 G. Guo, K. Gong, B. Wohlfeld, K. Hatanpaa, D. Zhao and A. Habib, *Cancer Res.*, 2015, **75**, 3436–3441.
  - 27 B. Alberts, A. Johnson, J. Lewis, D. Morgan, M. Raff, K. Roberts and P. Walter, *Molecular Biology of the Cell*, Garland Science, Taylor& Francis Group, New York, 6th edn., 2015.
  - 28 D. G. Evans, *Med. (United Kingdom)*, 2016, **44**, 65–68.

- 29 L. Villanova, S. Careccia, R. De Maria and M. E. Fiori, *Int. J. Mol. Sci.*, 2018, **19**, 958–972.
- 30 S. Elmore, *Toxicol. Pathol.*, 2007, **35**, 495–516.
- 31 Y. Shi, *Protein Sci.*, 2004, **13**, 1979–1987.
- 32 J. W. Shay and W. E. Wright, *Nat. Rev. Mol. Cell Biol.*, 2000, **1**, 72–76.
- 33 R. Leão, J. D. Apolónio, D. Lee, A. Figueiredo, U. Tabori and P. Castelo-Branco, *J. Biomed. Sci.*, 2018, **25**, 1–12.
- 34 A. Nabetami and F. Ishikawa, *J. Biochem.*, 2011, **149**, 5–14.
- 35 N. Nishida, *Vasc. Health Risk Manag.*, 2006, **2**, 213–219.
- 36 T. Khan and P. Gurav, *Front. Pharmacol.*, 2018, **8**, 1–14.
- 37 K. Greish, *Methods Mol. Biol.*, 2010, **624**, 25–37.
- 38 J. Fang, H. Nakamura and H. Maeda, *Adv. Drug Deliv. Rev.*, 2011, **63**, 136–151.
- 39 T. N. Seyfried and L. C. Huysentruyt, *Crit. Rev. Oncog.*, 2013, **18**, 43–73.
- 40 N. Vargas-Rondón, V. E. Villegas and M. Rondón-Lagos, *Cancers (Basel)*, 2018, **10**, 1–21.
- 41 Tumour Suppressor Genes, <https://www.cancer.org/cancer/cancer-causes/genetics/genes-and-cancer/oncogenes-tumor-suppressor-genes.html>, (accessed 18 January 2019).
- 42 A. Bolano, Aerobic Cellular Respiration: Definition And Steps, <https://sciencetrends.com/aerobic-cellular-respiration-definition-and-steps/>, (accessed 18 January 2019).
- 43 K. O. Alfarouk, D. Verduzco, C. Rauch, A. K. Muddathir, A. H. H. Bashir, G. O. Elhassan, M. E. Ibrahim, J. D. P. Orozco, R. A. Cardone, S. J. Reshkin and S. Harguindey, *Oncoscience*, 2014, **1**, 777.
- 44 M. V. Liberti, J. W. Locasale, C. Biology and C. Biology, *Trends Biochem. Sci.*, 2017, **41**, 211–218.
- 45 J. Fernandez-De-Cossio-Diaz and A. Vazquez, *Sci. Rep.*, 2017, **7**, 1–8.
- 46 S. M. Candeias and U. S. Gaipl, *Anticancer. Agents Med. Chem.*, 2015, **16**, 101–107.
- 47 D. Mittal, M. M. Gubin, R. D. Schreiber and M. J. Smyth, *Curr. Opin. Immunol.*, 2014, **27**, 16–25.
- 48 K. Grønbaek, C. Hother and P. A. Jones, *APMIS*, 2007, **115**, 1039–1059.

- 49 G. Song, L. Cheng, Y. Chao, K. Yang and Z. Liu, *Adv. Mater.*, 2017, **29**, 1–26.
- 50 L. Torrisi, *Radiat. Eff. Defects Solids*, 2018, **173**, 719–728.
- 51 T. Robak and M. Kasznicki, *Leukemia*, 2002, **16**, 1015–1027.
- 52 B. T. Oronsky, T. Reid, S. J. Knox and J. Scicinski, *Transl. Oncol.*, 2012, **5**, 226–229.
- 53 S. H. van Rijt and P. J. Sadler, *Drug Discov. Today*, 2009, **14**, 1089–1097.
- 54 K. D. Mjos and C. Orvig, *Chem. Rev.*, 2014, **114**, 4540–4563.
- 55 M. Zaki, F. Arjmand and S. Tabassum, *Inorganica Chim. Acta*, 2016, **444**, 1–22.
- 56 J. P. Becker, J. Weiss and D. Theile, *Toxicol. Lett.*, 2014, **225**, 43–47.
- 57 M. Crespo, *J. Organomet. Chem.*, 2019, **879**, 15–26.
- 58 M. D. Hall, C. Martin, D. J. P. Ferguson, R. M. Phillips, T. W. Hambley and R. Callaghan, *Biochem. Pharmacol.*, 2004, **67**, 17–30.
- 59 D. Gibson, *J. Inorg. Biochem.*, 2019, **191**, 77–84.
- 60 C. G. Hartinger, S. Zorbas-Seifried, M. A. Jakupec, B. Kynast, H. Zorbas and B. K. Keppler, *J. Inorg. Biochem.*, 2006, **100**, 891–904.
- 61 M. Groessl, C. G. Hartinger, K. Poleć-Pawlak, M. Jarosz, P. J. Dyson and B. K. Keppler, *Chem. Biodivers.*, 2008, **5**, 1609–1614.
- 62 G. K. Gransbury, P. Kappen, C. J. Glover, J. N. Hughes, A. Levina, P. A. Lay, F. Musgrave and H. H. Harris, *Metallomics*, 2016, **8**, 762–773.
- 63 S. Thota, D. A. Rodrigues, D. C. Crans and E. J. Barreiro, *J. Med. Chem.*, 2018, **61**, 5805–5821.
- 64 P. B. Tchounwou, C. Newsome, J. Williams and K. Glass, *Met. Ions Biol. Med.*, 2008, **10**, 285–290.
- 65 B. Ashish, K. Neeti and K. Himanshu, *Res. J. Recent Sci.*, 2013, **2**, 58–67.
- 66 M. F. Primik, G. Mühlgassner, M. A. Jakupec, O. Zava, P. J. Dyson, V. B. Arion and B. K. Keppler, *Inorg. Chem.*, 2010, **49**, 302–311.
- 67 A. Sîrbu, O. Palamarciuc, M. V Babak, M. J. Lim, K. Ohui, E. Enyedy, S. Shova, D. Darvasiová, P. Rapta, W. H. Ang and V. B. Arion, *Dalt. transactions*, 2017, **46**, 3833–3847.
- 68 F. Bacher, É. A. Enyedy, N. V Nagy, A. Rockenbauer, G. M. Bognár, R. Trondl, M. S. Novak, E.

- Klapproth and V. B. Arion, *Inorg. Chem.*, 2013, **52**, 8895–8908.
- 69 L. K. Filak, G. Mühlgassner, M. A. Jakupec, P. Heffeter, W. Berger, V. B. Arion and B. K. Keppler, *J. Biol. Inorg. Chem.*, 2010, **15**, 903–918.
- 70 A. Dobrov, S. Göschl, M. A. Jakupec, A. Popović-Bijelić, A. Gräslund, P. Rapta and V. B. Arion, *Chem. Commun.*, 2013, **49**, 10007–10009.
- 71 V. B. Arion, A. Dobrov, S. Göschl, M. A. Jakupec, B. K. Keppler and P. Rapta, *Chem. Commun.*, 2012, **48**, 8559–8561.
- 72 A. A. Alkhateeb and J. R. Connor, *Biochim. Biophys. Acta - Rev. Cancer*, 2013, **1836**, 245–254.
- 73 C. Hershko, *Food Nutr. Bull.*, 2007, **28**, 500–509.
- 74 N. V Gerbeleu, Y. A. Simonov, V. B. Arion, V. M. Leovac, K. I. Turta, K. M. Indrichan, D. I. Gradinaru, V. E. Zavodnik and T. I. Malinovskii, *Inorg. Chem.*, 1992, **31**, 3264–3268.
- 75 A. Enyedy, M. F. Primik, C. R. Kowol, V. B. Arion, T. Kiss and B. K. Keppler, *Dalt. Trans.*, 2011, **40**, 5895–5905.
- 76 C. Karthaler-Benbakka, D. Groza, K. Kryeziu, V. Pichler, A. Roller, W. Berger, P. Heffeter and C. R. Kowol, *Angew. Chemie*, 2014, **53**, 12930–12935.
- 77 S. Valihadi, P. Heffeter, M. Jakupec, R. Marculescu, W. Berger, K. Rappersberger and B. K. Keppler, *Melanoma Res.*, 2009, **19**, 283–293.
- 78 E. G. Koutsandrea, M. A. Foustieris and S. S. Nikolaropoulos, *Heterocycl. Commun.*, 2012, **18**, 169–179.
- 79 E. A. Sausville, D. Zaharevitz, R. Gussio, L. Meijer, M. Louarn-Leost, C. Kunick, R. Schultz, T. Lahusen, D. Headlee, S. Stinson, S. G. Arbuck and A. Senderowicz, *Pharmacol. Ther.*, 1999, **82**, 285–292.
- 80 A. Putey, F. Popowycz, Q. T. Do, P. Bernard, S. K. Talapatra, F. Kozielski, C. M. Galmarini and B. Joseph, *J. Med. Chem.*, 2009, **52**, 5916–5925.
- 81 V. Pons, S. Beaumont, M. E. Tran Huu Dau, B. I. Iorga and R. H. Dodd, *ACS Med. Chem. Lett.*, 2011, **2**, 565–570.
- 82 T. A. Chohan, A. Qayyum, K. Rehman, M. Tariq and M. S. H. Akash, *Biomed. Pharmacother.*, 2018, **107**, 1326–1341.
- 83 M. Ingham and G. K. Schwartz, *J. Clin. Oncol.*, 2017, **35**, 2949–2959.

- 84 M. E. Law, P. E. Corsino, S. Narayan and B. K. Law, *Mol. Pharmacol.*, 2015, **88**, 846–852.
- 85 G. Chashoo and A. K. Saxena, *J. Cancer Sci. Ther.*, 2014, **6**, 488–496.
- 86 P. Devlal and A. Singh, *Pharma Innov. J.*, 2017, **6**, 843–857.
- 87 A. Zetterberg, O. Larsson and K. Wiman, *Curr. Opin. Cell Biol.*, 1995, **7**, 835–842.
- 88 I. Potapov, J. Latukka, J. Kim, P. Luukko, K. Aalto-Setälä and E. Rääänen, *Sci. Rep.*, 2018, **8**, 14992–15002.
- 89 S. Nachimuthu, M. D. Assar and J. M. Schussler, *Ther. Adv. Drug Saf.*, 2012, **3**, 241–253.
- 90 S. Banerjee, D. J. Hwang, W. Li and D. D. Miller, *Molecules*, 2016, **21**, 1468–1486.
- 91 Q. Lai, Y. Wang, R. Wang, W. Lai, L. Tang, Y. Tao, Y. Liu, R. Zhang, L. Huang, H. Xiang, S. Zeng, L. Gou, H. Chen, Y. Yao and J. Yang, *Eur. J. Med. Chem.*, 2018, **156**, 162–179.
- 92 L. Li, S. Jiang, X. Li, Y. Liu, J. Su and J. Chen, *Eur. J. Med. Chem.*, 2018, **151**, 482–494.
- 93 Y. Lu, J. Chen, M. Xiao, W. Li and D. D. Miller, *Pharm. Res.*, 2012, **29**, 2943–2971.
- 94 R. Visconti and D. Grieco, *Endocr. Relat. Cancer*, 2017, **24**, T107–T117.
- 95 R. Berges, N. Baeza-Kallee, E. Tabouret, O. Chinot, M. Petit, A. Kruczynski, D. Figarella-Branger, S. Honore and D. Braguer, *Oncotarget*, 2014, **5**, 12769–12787.
- 96 J. Shi and T. J. Mitchison, *Endocr. Relat. Cancer*, 2017, **24**, 83–96.
- 97 J. J. Field, A. B. Waight and P. D. Senter, *Proc. Natl. Acad. Sci.*, 2014, **111**, 13684–13685.
- 98 M. Younas, C. Hano, N. Giglioli-Guivarc’H and B. H. Abbasi, *RSC Adv.*, 2018, **8**, 29714–29744.
- 99 X. Lei, M. Chen, M. Huang, X. Li, C. Shi, D. Zhang, L. Luo, Y. Zhang, N. Ma, H. Chen, H. Liang, W. Ye and D. Zhang, *Theranostics*, 2018, **8**, 384–398.
- 100 O. C. F. Orban, R. S. Korn, D. Benítez, A. Medeiros, L. Preu, N. Loaëc, L. Meijer, O. Koch, M. A. Comini and C. Kunick, *Bioorganic Med. Chem.*, 2016, **24**, 3790–3800.
- 101 S. E. Lee, S. J. Lee and C. H. Cheon, *Synth.*, 2017, **49**, 4247–4253.
- 102 J. Ryczak, M. Papini, A. Lader, A. Nasereddin, D. Kopelyanskiy, L. Preu, C. L. Jaffe and C. Kunick, *Eur. J. Med. Chem.*, 2013, **64**, 396–400.
- 103 C. Schultz, A. Link, M. Leost, D. W. Zaharevitz, R. Gussio, E. A. Sausville, L. Meijer and C. Kunick, *J. Med. Chem.*, 1999, **42**, 2909–2919.

- 104 D. W. Zaharevitz, R. Gussio, M. Leost, A. M. Senderowicz, T. Lahusen, C. Kunick, L. Meijer and E. A. Sausville, *Cancer Res.*, 1999, **59**, 2566–2569.
- 105 A. Putey, L. Joucla, L. Picot, T. Besson and B. Joseph, *Tetrahedron*, 2007, **63**, 867–879.
- 106 L. Keller, S. Beaumont, J. M. Liu, S. Thoret, J. S. Bignon, J. Wdzieczak-Bakala, P. Dauban and R. H. Dodd, *J. Med. Chem.*, 2008, **51**, 3414–3421.
- 107 J. Garbarino, N. Troncoso, G. Frasca, V. Cardile and A. Russo, *Nat. Prod. Commun.*, 2008, **3**, 2095–2098.
- 108 C. Ma, L. Shi, Y. Huang, L. Shen, H. Peng, X. Zhu and G. Zhou, *Biomater. Sci.*, 2017, **5**, 494–501.
- 109 W. F. Schmid, S. Zorbas-Seifried, R. O. John, V. B. Arion, M. A. Jakupec, A. Roller, M. Galanski, I. Chiorescu, H. Zorbas and B. K. Keppler, *Inorg. Chem.*, 2007, **46**, 3645–3656.
- 110 W. F. Schmid, R. O. John, G. Mühlgassner, P. Heffeter, M. A. Jakupec, M. Galanski, W. Berger, V. B. Arion and B. K. Keppler, *J. Med. Chem.*, 2007, **50**, 6343–6355.
- 111 W. F. Schmid, R. O. John, V. B. Arion, M. A. Jakupec and B. K. Keppler, *Organometallics*, 2007, **26**, 6643–6652.
- 112 R. Wijtman, M. K. Vink, H. E. Schoemaker, F. L. van Delft, R. H. Blaauw and F. P. Rutjes, *Synthesis (Stuttg.)*, 2004, **2004**, 641–662.
- 113 A. N. Matralis and A. P. Kourounakis, *ACS Med. Chem. Lett.*, 2019, **10**, 98–104.
- 114 A. Dobrov, V. B. Arion, N. Kandler, W. Ginzinger, M. A. Jakupec, A. Ruffinowska, N. G. von Keyserlingk, M. Galanski, C. Kowol and B. K. Keppler, *Inorg. Chem.*, 2006, **45**, 1945–1950.
- 115 G. Mühlgassner, C. Bartel, W. F. Schmid, M. A. Jakupec, V. B. Arion and B. K. Keppler, *J. Inorg. Biochem.*, 2012, **116**, 180–187.
- 116 V. Polshettiwar and M. P. Kaushik, *Tetrahedron Lett.*, 2004, **45**, 6255–6257.
- 117 A. W. Addison, T. N. Rao, J. Reedijk, J. Van Rijn and G. C. Verschoor, *Dalt. Trans.*, 1984, 1349–1356.
- 118 M. N. M. Milunović, A. Dobrova, G. Novitchi, N. Gligorijević, S. Radulović, J. Kožiček, P. Rapt, É. A. Enyedy and V. B. Arion, *Eur. J. Inorg. Chem.*, 2017, 4773–4783.
- 119 K. Ohui, E. Afanasenko, F. Bacher, R. L. X. Ting, A. Zafar, N. Blanco-Cabra, E. Torrents, O. Dömötör, N. V. May, D. Darvasiova, É. A. Enyedy, A. Popović-Bijelić, J. Reynison, P. Rapt, M. V. Babak, G. Pastorin and V. B. Arion, *J. Med. Chem.*, 2019, **62**, 512–530.

## 7. Supplementary Information

### 7.1. Zusammenfassung

Die Behandlung von Krebs wurde im letzten Jahrhundert um viele Facetten erweitert. Die Grundlage für die metallbasierte Krebstherapie legte die Entdeckung der zytotoxischen Wirkung von Cisplatin. Der Erfolg von Cisplatin führte zur Entwicklung weiterer Platin(II)-Therapeutika. Trotz der vielen Vorteile, die diese Medikamente mit sich bringen, besitzen sie auch gravierende Nachteile, wie Nebenwirkungen und Resistenzen. Mit der Entdeckung von Ruthenium(II)- und Ruthenium(III)-Therapeutika wurden die Nebenwirkungen reduziert und auch Resistenzen umgangen. Obwohl auch diese Chemotherapeutika gute Wirkung zeigen, ist der Bedarf an neuen Wirkstoffen ungebremst, um Krebs gezielt zu bekämpfen.

Cyclin-abhängige Kinasen (CDKs) und Tubuline sind zwei Proteinfamilien von essentieller Bedeutung für den Zellzyklus. Es gibt eine Vielzahl an CDKs, welche den Zellzyklus kontrollieren. CDKs sind in karzinogenen Zellen oft mutiert, was zu einer unkontrollierten Zellteilung und zu einer Akkumulation von Mutationen führt. Deshalb kann eine gezielte Inhibierung dieser mutierten Proteine den Zellzyklus stilllegen. Tubulin spielt bei der Mitose eine tragende Rolle. Die Polymerisation und Depolymerisation der Untereinheiten kann ein Ziel für Medikamente sein, da sowohl eine Stabilisierung der noch nicht polymerisierten Untereinheiten, als auch eine Stabilisierung des Polymerisierten Komplexes die Zellteilung stört.

Mit der Entdeckung von Paullonen und deren Derivaten konnte man CDKs gezielt attackieren. Jedoch wiesen diese Moleküle eine niedrige Wasserlöslichkeit auf, welche durch Komplexbildung, mit zum Beispiel Kupfer, deutlich erhöht werden konnte. Latonduine mit einer Indoleinheit, ein Derivat von Paullonen, zeigten starke Inhibierung von Tubulin, jedoch sind auch sie schlecht wasserlöslich.

In dieser Arbeit wurden Latonduin-Derivate, auf Basis von 5,8-dihydroindolo[2,3-*d*][2]benzazepin-7(6*H*)-onen, synthetisiert und modifiziert, sodass passende Bindungsstellen für Übergangsmetalle (Kupfer(II) und Eisen(III)) generiert werden konnten. Die Charakterisierung der Liganden wurde mit ein- und zwei-dimensionaler  $^1\text{H}$  und  $^{13}\text{C}$  NMR-Spektroskopie durchgeführt. Die neuen Komplexe wurden mittels UV-vis und IR-Spektroskopie und Elementaranalyse charakterisiert. Des Weiteren wurde deren

elektrochemisches Verhalten analysiert. Erste Zelltests lassen ein hohes Potential für die Weiterentwicklung dieser Medikamente vermuten.

## 7.2. Abstract

In the past century the treatment of cancer has improved rapidly. The metal based anticancer therapy was set by cisplatin. This drug and many other platinum(II) drugs were and are currently used to treat cancer. Nevertheless, these drugs show severe side effects. More promising are ruthenium(II)- or ruthenium(III)-based drugs to further reduce side effects and overcome acquired resistance against cisplatin. Although these drugs work well, improvement is still needed in synthesising targeted drugs.

Two major protein groups controlling the cell's proliferation are cyclin-dependent kinases (CDKs) and tubulins. Many different sub-classes of CDKs are known. Some of them are sentinels of the cell cycle allowing the cell to proliferate. This enzyme is corrupted in cancer, thus, no monitoring for damaged DNA can be conducted, allowing the cell to proliferate with an accumulation of mutations. Therefore, targeted inhibition of these aberrant proteins may lead to cell cycle arrest. Tubulin plays the main role during mitosis. It polymerises at the beginning and depolymerises when the separation of chromosomes is finished. Thus, targeted inhibition of either the polymerisation or depolymerisation of this protein complex will stop the cell from proliferating.

With the discovery of the highly cytotoxic effects of paullones and its derivatives, CDKs could be targeted to eliminate aberrant cells. The drawback of these molecules is their low aqueous solubility, which was successfully improved by complex formation with different metals like copper(II) or iron(III). Latonduine derivatives bearing an indole moiety have promising tubulin inhibitory properties, but suffer from the same disadvantage as paullones.

In this work, latonduine derivatives, namely 5,8-dihydroindolo[2,3-*d*][2]benzazepine-7(6*H*)-ones, were synthesised and modified by creating suitable metal binding sites for accommodation of copper(II) and of iron(III). The ligands were characterised by one- and two-dimensional  $^1\text{H}$  and  $^{13}\text{C}$  NMR spectroscopy, UV-vis and IR spectroscopy, elemental analysis and electrochemical techniques. Preliminary cytotoxicity assays will indicate high potential for their further development as anticancer drugs.